Article

Cell Reports

Dnmt3bas coordinates transcriptional induction and alternative exon inclusion to promote catalytically active Dnmt3b expression

Graphical abstract

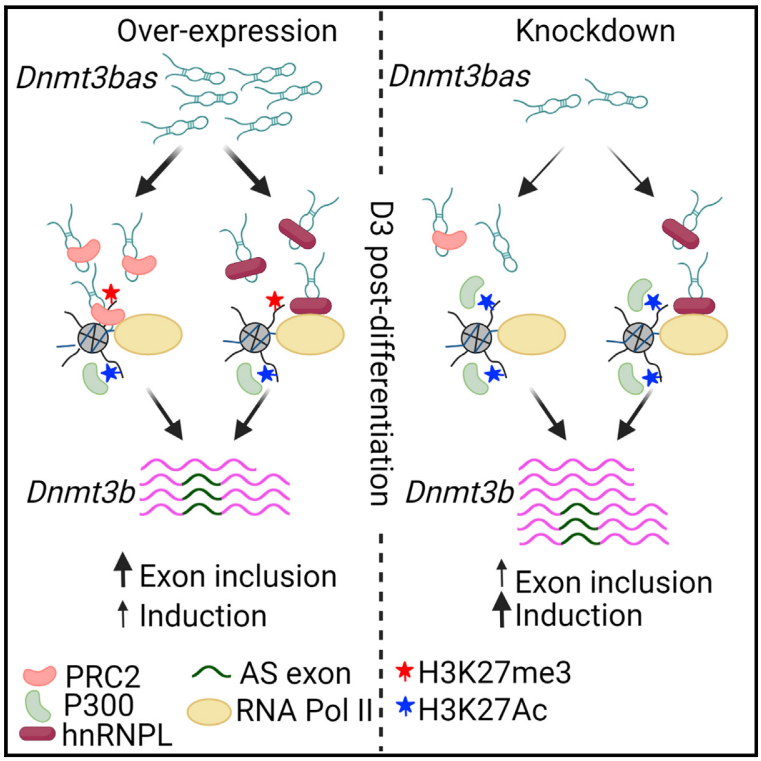

Authors

Mohd Saleem Dar, Isaiah K. Mensah, Ming He, ..., Hern J. Tan, Mark C. Hall, Humaira Gowher

Correspondence

hgowher@purdue.edu

In brief

Dar et al. report the regulatory role of *Dnmt3bas* lncRNA and *cis*-regulatory regions in *Dnmt3b* expression. By interacting with and recruiting the PRC2 complex and hnRNPL to the *Dnmt3b* promoter, *Dnmt3bas* regulates transcriptional induction and alternative splicing of *Dnmt3b*, dictating the prevalence of catalytically active DNMT3B, required for global *de novo* methylation.

Highlights

- *Dnmt3bas* is a spliced and polyadenylated lncRNA
- *Dnmt3bas* fine-tunes *Dnmt3b* transcriptional induction by regulating PRC2 activity
- *Dnmt3bas* promotes exon inclusion to express catalytically active *Dnmt3b1* isoform
- *Dnmt3bas* recruits hnRNPL and coordinates transcription with alternative splicing

Dar et al., 2023, Cell Reports *42*, 112587
June 27, 2023 © 2023 The Author(s).
https://doi.org/10.1016/j.celrep.2023.112587

CellPress

Cell Reports

CellPress
OPEN ACCESS

Article

Dnmt3bas coordinates transcriptional induction and alternative exon inclusion to promote catalytically active Dnmt3b expression

Mohd Saleem Dar,[1] Isaiah K. Mensah,[1] Ming He,[1] Sarah McGovern,[1] Ikjot Singh Sohal,[2,3] Hannah Christian Whitlock,[1] Nina Elise Bippus,[1] Madison Ceminsky,[1] Martin L. Emerson,[1] Hern J. Tan,[1] Mark C. Hall,[1,2] and Humaira Gowher[1,2,4,*]

[1]Department of Biochemistry, Purdue University, West Lafayette, IN 47907, USA
[2]Purdue University Center for Cancer Research, Purdue University, West Lafayette, IN 47907, USA
[3]Department of Biological Sciences, Purdue University, West Lafayette, IN 47907, USA
[4]Lead contact
*Correspondence: hgowher@purdue.edu
https://doi.org/10.1016/j.celrep.2023.112587

SUMMARY

Embryonic expression of DNMT3B is critical for establishing *de novo* DNA methylation. This study uncovers the mechanism through which the promoter-associated long non-coding RNA (lncRNA) *Dnmt3bas* controls the induction and alternative splicing of *Dnmt3b* during embryonic stem cell (ESC) differentiation. *Dnmt3bas* recruits the PRC2 (polycomb repressive complex 2) at *cis*-regulatory elements of the *Dnmt3b* gene expressed at a basal level. Correspondingly, *Dnmt3bas* knockdown enhances *Dnmt3b* transcriptional induction, whereas overexpression of *Dnmt3bas* dampens it. *Dnmt3b* induction coincides with exon inclusion, switching the predominant isoform from the inactive *Dnmt3b6* to the active *Dnmt3b1*. Intriguingly, overexpressing *Dnmt3bas* further enhances the *Dnmt3b1*:*Dnmt3b6* ratio, attributed to its interaction with hnRNPL (heterogeneous nuclear ribonucleoprotein L), a splicing factor that promotes exon inclusion. Our data suggest that *Dnmt3bas* coordinates alternative splicing and transcriptional induction of *Dnmt3b* by facilitating the hnRNPL and RNA polymerase II (RNA Pol II) interaction at the *Dnmt3b* promoter. This dual mechanism precisely regulates the expression of catalytically active DNMT3B, ensuring fidelity and specificity of *de novo* DNA methylation.

INTRODUCTION

During mammalian development, epigenetic reprogramming, which involves global erasure and reestablishment of DNA methylation, facilitates the acquisition of epigenetic plasticity and limits the inheritance of acquired epimutations.[1] DNA methylation is reset by the *de novo* methylation activity of DNMT3A and DNMT3B DNA methyltransferases. In mice, homozygous knockout of *dnmt3a* and *dnmt3b* is embryonic lethal,[2,3] and *Dnmt3b*$^{-/-}$ ESCs (murine embryonic stem cells) show defective differentiation potential and loss of DNA methylation at specific regulatory elements and minor satellite repeats, which are the preferred targets of the *Dnmt3b* enzyme.[2,4,5] *Dnmt3b* is dynamically expressed during development, with the highest expression restricted to the inner mass cells from embryonic day 4.5 (E4.5) to E8.5, after which it is strongly downregulated in somatic cell lineages.[2,6,7] During differentiation of naive pluripotent mouse ESCs (2i-ESCs), the transcript levels of *Dnmt3b* increase substantially within 2–3 days, after which the *Dnmt3b* gene is completely repressed.[8–10] This is akin to the dynamic expression of *Dnmt3b* during early embryogenesis, making it an ideal model system to study its regulation.

Dnmt3b is transcribed in more than 30 alternatively spliced isoforms, although only a few have been detected at the protein level.[11,12] Several of these isoforms are catalytically inactive due to the loss of key catalytic residues. The two major isoforms expressed in normal cells are *Dnmt3b1* and *Dnmt3b6*. The exclusion of exons 22 and 23 results in the loss of a significant part of the target recognition region in the *Dnmt3b6* transcript, thus rendering the protein enzymatically inactive. However, DNMT3B6 has been shown to interact and allosterically activate the full-length catalytically active enzyme DNMT3B1.[12–17] Aberrant expression and splicing of *DNMT3B* are linked to the loss of methylation at oncogenes and repetitive elements in diverse cancers, including colorectal, lung, and breast cancers.[18–21] Several observations indicate that the highly regulated spatiotemporal expression and alternative splicing of *DNMT3B* are critical for cell differentiation, homeostasis, and survival.[3,22] Despite the breadth of evidence supporting the critical role of *DNMT3B* in differentiation and cell identity, little is known about the mechanisms that control its transcription.

Transcription is controlled by the concerted activity of the transcriptional coactivator complex and a permissive chromatin environment at its *cis*-regulatory elements. Additionally,

This is an open access article under the CC BY-NC-ND license (http://creativecommons.org/licenses/by-nc-nd/4.0/).

divergent long non-coding RNAs (lncRNAs) regulate the expression of the nearby protein-coding genes, including those crucial for normal development. lncRNAs such as HOTAIR,[23] Kcnq1ot1,[24] Air,[25] Evx1as,[26] and Evf2as[27] are coordinately transcribed with a protein-coding gene such that the pair is expressed from one transcriptional locus.[28] Most lncRNAs are transcribed by RNA polymerase II (RNA Pol II), and many undergo capping, splicing, and polyadenylation.[29–31] In addition, lncRNAs interact with other chromatin proteins and regulate the activation and silencing of genes.[32–36] Transcription regulation by lncRNAs can be mediated by the act of transcription (in *cis*), which creates a chromatin environment that influences the expression of the neighboring gene.[37] The *trans* mechanisms involve the activity of the transcript, which may guide the recruitment of chromatin-modifying complexes such as PRC2.[23,32,38–46] lncRNAs that bind PRC2 include Airn, Kcnqtlot1, ANRASSF1, and COLDAIR,[23,29,43,47–50] mediating the formation of repressive chromatin structure at PRC2 target regions. Furthermore, PRC2 can bind lncRNAs by recognizing short tracts of Gs and G-quadruplexes, ubiquitously present in the transcriptome.[51–53]

A divergently expressed antisense transcript, *Dnmt3bas*, initiates 1 kb downstream of the *Dnmt3b* promoter (Gencode Transcript: ENSMUST00000124988.1 from GENCODE VM23 Comprehensive Transcript Set). Our study here characterized *Dnmt3bas* as a promoter-associated divergent lncRNA, expressed coordinately with *Dnmt3b* mRNA. Mechanistically, *Dnmt3bas* acts in *trans,* interacts with PRC2 and hnRNPL, and regulates the induction and alternative splicing of *Dnmt3b*. We show that in undifferentiated 2i-ESCs, *Dnmt3b* is expressed at a low basal level and primarily as *Dnmt3b6*, the catalytically inactive isoform. The expression of Dnmt3b is strongly induced in response to the differentation signal and is, interestingly, accompanied by exon inclusion, which promotes the expression of the catalytically active *Dnmt3b1* as the major isoform. As differentiation proceeds, *Dnmt3b* expression is downregulated. During ESC differentiation, a coordinated yet contrasting expression pattern of *Dnmt3b* and *Dnmt3bas* was observed, with the *Dnmt3b* pattern mimicking the expression of *Dnmt3b* observed *in vivo*. The chromatin modification state of proximal and distal enhancers and enhancer-promoter looping complemented the *Dnmt3b* transcriptional state. Whereas we observed no discernable effect of the downregulation (knockdown [KD]) or overexpression (OE) of *Dnmt3bas* on *Dnmt3b* basal expression, the transcriptional induction of *Dnmt3b* was decreased in *Dnmt3bas* OE cells and increased in *Dnmt3bas* KD cells. Interestingly, the undifferentiated OE cells showed an increase in H3K27me3 at the *cis*-regulatory elements, suggesting the role of *Dnmt3bas* in regulating PRC2 activity at these sites. Additionally, higher enrichment of H3K27Ac and an increased interaction frequency between enhancer and promoter were observed in the KD cells post-differentiation. In *Dnmt3bas* OE cells, we also observed increased exon inclusion, resulting in a higher *Dnmt3b1*:*Dnmt3b6* ratio. Our systematic experimental analysis determined the splicing factor hnRNPL as the binding partner of *Dnmt3bas* that facilitates exon inclusion during transcriptional induction of *Dnmt3b*.

Overall, this comprehensive study describes a mechanism by which a promoter-associated lncRNA, *Dnmt3bas*, coordinates transcriptional induction and alternative splicing of an essential developmental gene and establishes the role of *cis*-regulatory elements in this process.

RESULTS

Transcriptional induction and alternative splicing of Dnmt3b

We adapted the serum-cultured murine ESCs (s-ESCs) to 2i media (2i-ESCs), demonstrated by an apparent increase in the naive pluripotency markers and downregulation of *Dnmt3a* and *Dnmt3b*, with the concomitant loss of DNA methylation genome-wide (Figures S1A–S1C). Next, the differentiation of 2i-ESCs was monitored by a change in the expression of pluripotency and differentiation markers by qRT-PCR (Figures S1D and S1E). Analysis of *Dnmt3b* expression showed a 10- to 15-fold increase, which peaks at day 3, followed by a substantial decrease that stays steady from day 4 to 6 post-differentiation (Figure 1A). Since *Dnmt3b* is expressed at a low basal level in 2i-ESCs, the induction is significantly higher than that observed during the differentiation of s-ESCs (Figure S1F).

Dnmt3b transcripts comprise two major alternatively spliced isoforms: *Dnmt3b1*, a full-length transcript, and a catalytically inactive *Dnmt3b6*, in which exons 22 and 23 are excluded.[12–17] RT-PCR was used to amplify both isoforms pre- and post-differentiation of ESCs (Figure 1B). As shown previously,[54] both isoforms are expressed equally in s-ESCs. Interestingly, in 2i-cultured ESCs, *Dnmt3b* mainly comprises the shorter isoform *Dnmt3b6*, indicating that exon exclusion is preferred during basal transcription of *Dnmt3b*. However, after induction, *Dnmt3b1* is expressed as the major isoform, indicating that the alternative splicing switches in favor of exon inclusion. Post-differentiation transcriptional repression is again accompanied by switching to exon exclusion, and *Dnmt3b6* is expressed as a major isoform in embryoid bodies (Figures 1B and S1G). These data suggest that in conjunction with transcriptional induction, the alternative exon inclusion/exclusion regulates the level of catalytically active DNMT3B, underscoring the critical role of this coordinated process.

The *cis*-regulatory elements in the *Dnmt3b* locus constitute a CpG island promoter and putative proximal and distal enhancer elements located about 0.3 and 8 kb upstream of the transcription start site (TSS), respectively (Figure S1H).[8,55,56] To determine the engagement of the putative distal enhancer in the regulation of *Dnmt3b* expression, we examined the enhancer-promoter (E-P) looping interaction pre- and post-differentiation in 2i-ESCs using a chromatin conformation capture (3C) assay.[57,58] We observed a strong and specific contact between the distal enhancer and promoter regions (E-P loop), which increased post-differentiation (Figure 1C). Moreover, the E-P loop interaction was prevalent in the undifferentiated 2i-ESCs when *Dnmt3b* was expressed at the basal level, suggesting that pre-positioning the enhancer next to the promoter enables a quick transcriptional response to the induction signal.

Based on the transcriptional state of the associated gene, enhancer regions acquire different chromatin modifications.

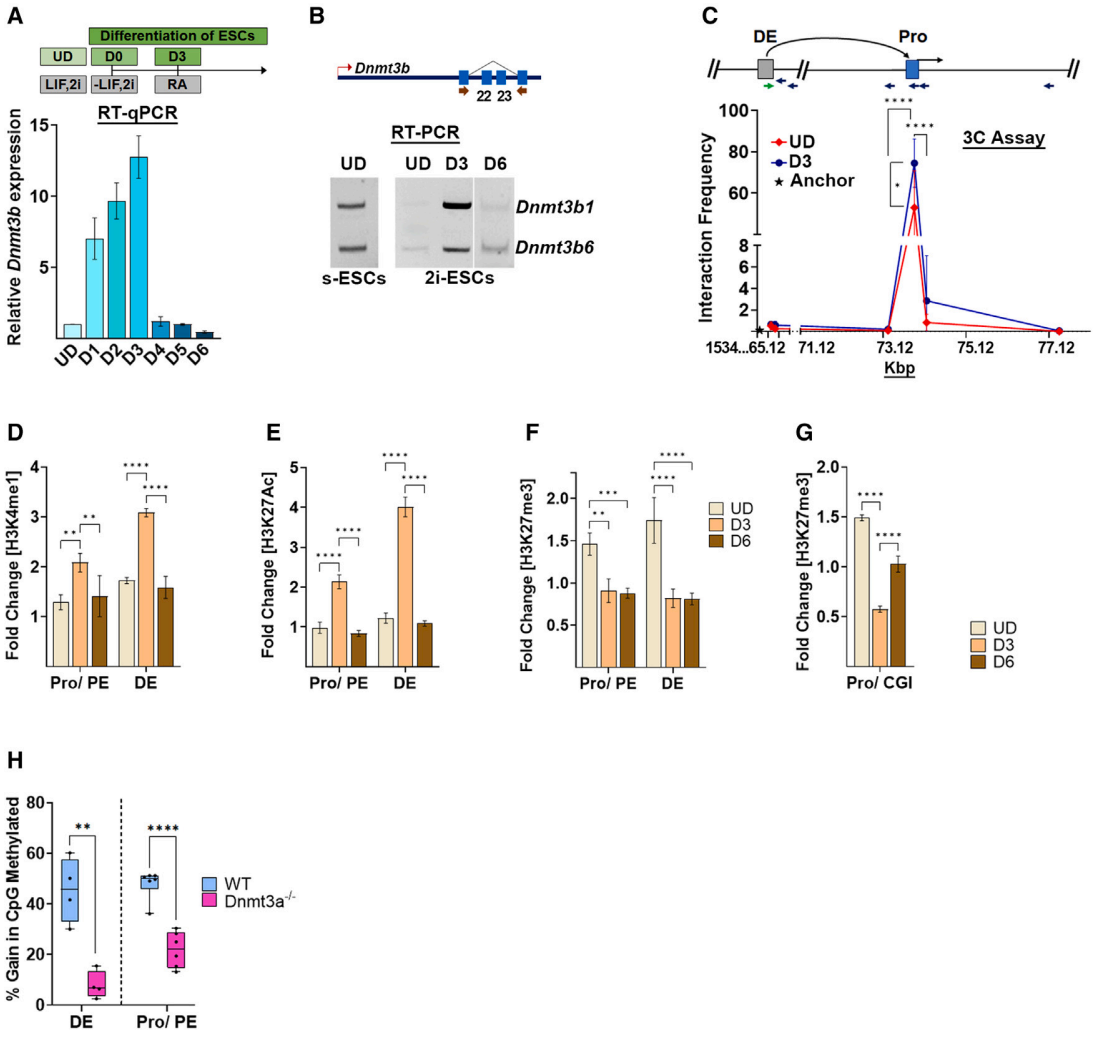

Figure 1. Proximal and distal enhancers regulate Dnmt3b induction

(A) qRT-PCR of Dnmt3b during 2i-ESC differentiation as illustrated. The threshold cycle (Ct) values were normalized to *Gapdh*, and expression is shown relative to that in UD cells.

(B) RT-PCR expression analysis in 2i-ESCs of *Dnmt3b1* and *Dnmt3b6* amplified in the same reaction mix by using primers flanking the AS exons. The illustration shows AS exons 22 and 23, and red arrows represent the primer's position to amplify around the AS exons of the Dnmt3b gene.

(C–G) Chromatin conformation capture (3C) assay shows an interaction of the distal enhancer (DE) with the region around the promoter of Dnmt3b. The illustration shows the arbitrary location of the DE and promoter (Pro) in the *Dnmt3b* locus. The 3C PCR primers (arrows) at the corresponding HaeIII sites are shown. Interaction frequency was calculated by qPCR analysis using the primer (green arrow) at the DE as an anchor (chromosome 2 [Chr2] position: 153,466,046). Plotted is the relative interaction frequency in arbitrary units of the Dnmt3b DE with regions around the six HaeIII sites. The x axis represents the Chr2 location (153,465,120–153,477,120) of these HaeIII sites.

(D–G) Chromatin immunoprecipitation (ChIP)-qPCR shows fold enrichment over input. Histone modifications at *Dnmt3b* regulatory elements (D) H3K4me1, (E) H3K27Ac, and (F and G) H3K27me3 in 2i-ESCs pre- and post-differentiation. Results are presented as normalized mean values ± SEM for n ≥3. p values were derived using the ANOVA test: *p < 0.05; **p < 0.01; ***p < 0.005. ****p < 0.0001.

(H) Bisulfite sequencing shows the percentage of CpG methylation at Dnmt3b regulatory elements in wild-type and *Dnmt3a*$^{-/-}$ cells. Bisulfite-treated DNA from wild-type and *Dnmt3a*$^{-/-}$ cells was sequenced using a high-throughput sequencing platform (Wide-seq), and Bismark software was used to analyze the data. The boxplot represents the range of the percentage of DNA methylation at various CpG sites in each target region. The median methylation at both targets is higher in KD cells compared with vector control (VC) cells. p values were calculated using Wilcoxon matched-pairs rank test: *p < 0.05; **p < 0.01; ***p < 0.005. See also Figure S1.

UD, undifferentiated; D1–D6, days post-induction of differentiation; ESCs, embryonic stem cells; s-ESCs, serum cultured ESCs; RA, retinoic acid; LIF, leukocyte inhibitory factor; 2i, signaling pathway inhibitors CHIR99021 and PD184352; PE, proximal enhancer; Pro, promoter; DE, distal enhancer; CGI, CpG island; WT, wild type; *Dnmt3b1*, Dnmt3b long isoform (exons 22 and 23 included); *Dnmt3b6*, Dnmt3b short isoform (exons 22 and 23 excluded).

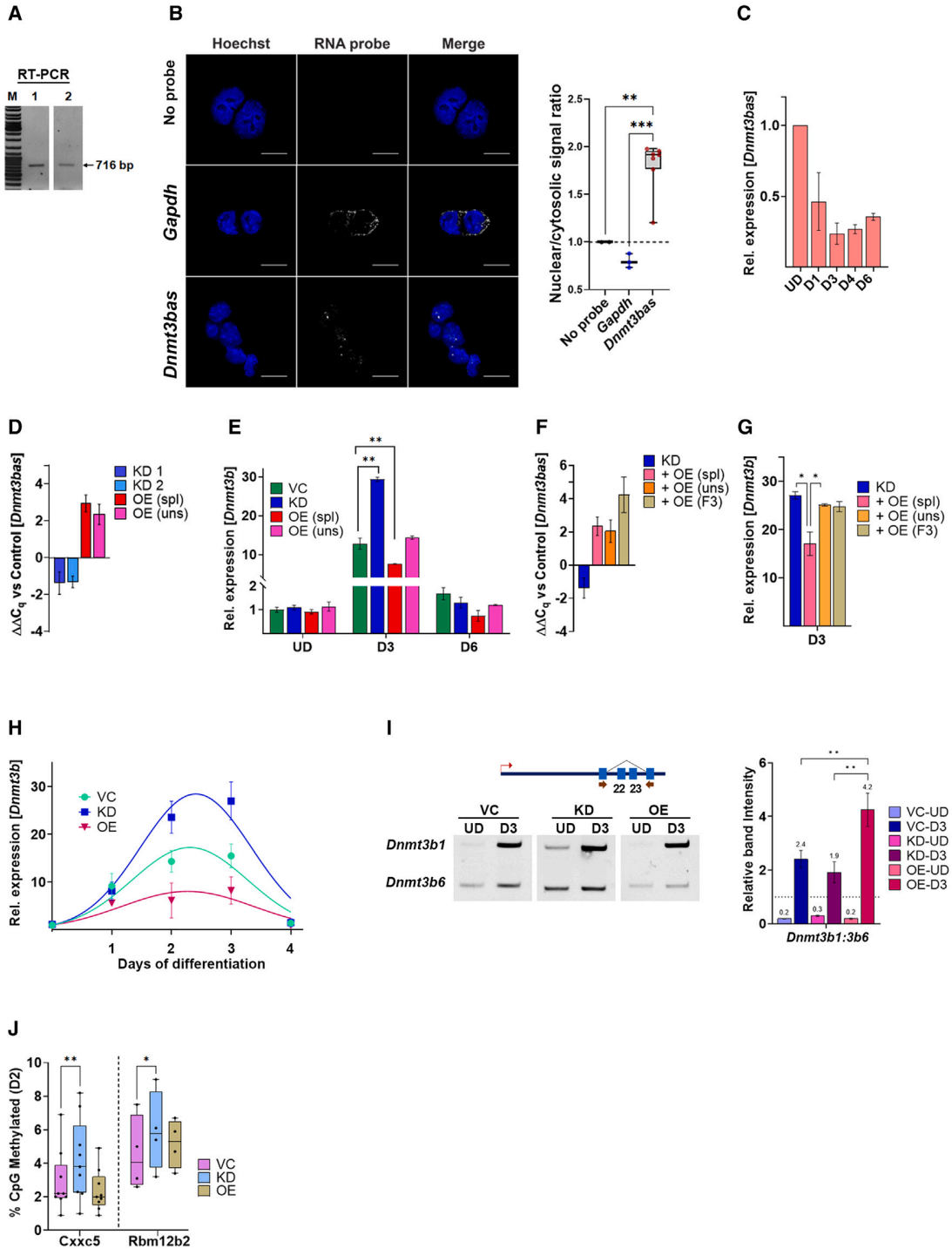

Figure 2. Spatiotemporal expression and alternative splicing of Dnmt3b in *Dnmt3bas*-manipulated ESCs

(A) Ethidium bromide-stained agarose gel. RT-PCR of *Dnmt3bas* using exonic (lane 1) and Oligo dT (lane 2) primers.

(B) Representative RNA-FISH confocal images of s-ESCs demonstrating nuclear enrichment of *Dnmt3bas* transcript. *Gapdh* was used as a control for cytosolic enrichment. The right bar graph shows the signal quantification. The nuclear and cytosolic signal was quantified, and the nuclear/cytosolic signal ratio was plotted for each RNA probe ($n \geq 3$). The ratio was normalized to unstained control. Ratio >1 demonstrates nuclear enrichment, and ratio <1 demonstrates cytosolic enrichment. p values were calculated using ANOVA: $^{**}p < 0.01$, $^{***}p < 0.001$.

(legend continued on next page)

We measured the enrichment of H3K4me1, H3K27Ac, and H3K27me3 at *Dnmt3b* regulatory regions pre- and post-differentiation by Chromatin immunoprecipitation (ChIP) assays. At day 3 post-differentiation, we observed an expected increase in H3K4me1 and H3K27Ac concomitant with enhancer activation and induction of *Dnmt3b* expression. *Dnmt3b* repression at day 6 post-differentiation was associated with a decrease in H3K4me1 and H3K27Ac at both proximal and distal enhancer regions (Figures 1D and 1E). In contrast, H3K27me3 at the proximal and distal enhancer regions was higher in undifferentiated (UD) 2i-ESCs and decreased post-differentiation at days 3 and 6 (Figure 1F). The *Dnmt3b* promoter also harbors a CpG island (CGI) around the TSS. It is noteworthy that whereas deacetylation of H3K27 is not succeeded by H3K27 methylation at proximal and distal enhancer sites, the CGI promoter region showed a significant recovery of H3K27me3 at day 6 post-differentiation, demonstrating that the PRC2-mediated mechanism maintains the repressed state of the *Dnmt3b* promoter (Figure 1G). H3 occupancy shows no significant difference in enrichment in various samples pre- and post-differentiation, further validating the significance of the observed chromatin modification changes (Figure S1I).

Previous studies have shown that during enhancer silencing, histone demethylation of H3K4me1 and deacetylation of H3K27Ac by the Lsd1-Mi2NuRD-complex poises the chromatin for DNMT3A-catalyzed DNA methylation.[59] Methylation-dependent qPCR (MD-qPCR) and bisulfite sequencing showed at distal and proximal enhancer regions a significant gain of DNA methylation (~50%), which was severely reduced in *Dnmt3a*$^{-/-}$ cells on day 6 post-differentiation (Figures 1H and S1J). Furthermore, as previously reported for strong CGIs, the DNA methylation levels decreased with increasing proximity to the *Dnmt3b* promoter CGI (Figure S1K). Overall, these data establish the mechanistic role of PRC2 and DNMT3A at the promoter and distal and proximal enhancers in regulating *Dnmt3b* expression during 2i-ESC differentiation.

Dnmt3bas regulates the induction and alternative splicing of Dnmt3b

The divergent antisense (*as*) lncRNA *Dnmt3bas* is a 2.8 kb transcript that initiates 800 bp downstream of the TSS in the *Dnmt3b* promoter. Based on the predicted exon-intron boundaries, we designed primers to capture potential spliced and polyadenylated forms of *Dnmt3bas* (Figure S2A). A unique band of nearly 716 bp, corresponding to the size of spliced *Dnmt3bas*, confirmed the splicing and polyadenylation of *Dnmt3bas* (Figure 2A). We used the RNA fluorescence *in situ* hybridization (RNA FISH) technique to detect *Dnmt3bas* transcripts in ESCs. As expected, the *Gapdh* mRNA was primarily localized in the cytoplasm, whereas the *Dnmt3bas* transcripts were mainly localized in a punctate pattern in the nucleus. Mostly one or two large and a few tiny puncta were observed in the nucleus, with no detectable signal in the cytoplasm (Figures 2B and S2N). The nuclear localization of *Dnmt3bas* was further confirmed by subcellular fractionation assays (Figure S2B).

We first asked if there is a correlation between the expression of *Dnmt3b* and *Dnmt3bas* during 2i medium adaptation and differentiation of ESCs. 2i medium adaptation was validated by confirming expected gene expression changes in the naive ESCs[9] (Figure S2C). Exon-specific primers were used to detect the expression of spliced *Dnmt3bas*, which also minimizes potential amplification from genomic DNA contamination in the RNA samples (Table S1). qRT-PCR specificity was ensured by the absence of signal in the NRT (no reverse transcriptase) control and by visualizing the amplified product as a single band on an agarose gel (Figure S2D). Expression analysis showed that whereas *Dnmt3b* was downregulated at passage 6 (P6) and maintained a basal level in 2i-ESCs, *Dnmt3bas* expression constantly increased during adaptation (Figure S2E). However, during 2i-ESC differentiation, the expression of *Dnmt3bas* was downregulated concomitantly with the induction of the *Dnmt3b* (Figures 1A and 2C).

The coordinated yet contrasting expression pattern of the *Dnmt3b*/*Dnmt3bas* pair suggests a potential role for *Dnmt3bas* in regulating *Dnmt3b* transcription. Therefore, we generated stable ESC lines expressing anti-*Dnmt3bas* short hairpin RNA (shRNA; KD1 and KD2) or overexpressing spliced and unspliced forms (spl and uns, respectively) of *Dnmt3bas* and adapted them to 2i medium (Figures S2F and S2G). *Dnmt3bas* KD1 and KD2 cells showed a significant reduction of *Dnmt3bas* by nearly 2.5-fold compared with the vector control (VC) cells. Conversely, *Dnmt3bas* OE cells showed nearly 8- to 9-fold higher expression

(C, D, and F) qRT-PCR analysis of *Dnmt3bas* expression (C) in 2i-ESCs pre- and post-differentiation; (D) in transgenic 2i-ESC lines expressing *Dnmt3bas* shRNA (KD1, KD2) or overexpressing spliced (OE spl) and unspliced (OE uns) transcripts of *Dnmt3bas*; and (F) in *Dnmt3bas* KD cells OE spl, uns, or truncated fragment of *Dnmt3bas* (F3 as in Figure 5). The Ct values were normalized to Gapdh, and expression is shown relative to that in VC cells set to 0.

(E and G) qRT-PCR analysis of *Dnmt3b* expression (E) in *Dnmt3bas*-manipulated transgenic 2i-ESCs and pre-and post-differentiation (G) in *Dnmt3bas* KD cells OE spl, uns, or truncated fragment of *Dnmt3bas* (F3).

(H) Dnmt3b expression in VC, OE, and KD cell lines was measured every 24 h post-differentiation. The data were fit to a non-linear regression in PRISM to estimate the time of the Dnmt3b induction peak. Results are presented as normalized mean values ± SEM. See also Figure S2. p values were derived from the ANOVA test or Student's t test: *$p < 0.05$; **$p < 0.01$; ***$p < 0.005$.

(I) RT-PCR expression analysis in 2i-ESCs of *Dnmt3b1* and *Dnmt3b6* as described in the Figure 1 legend. The bar graph shows the ratio of quantified band intensity *Dnmt3b1* and *Dnmt3b6* from at least 3 gels.

(J) DNA methylation analysis using Bis-Seq. Bisulfite-treated genomic DNA from day 2 differentiated cells was used to PCR amplify two Dnmt3b-specific target regions, CXXC5: chr18: 35,858,578:35,858,863 and Rbm12b2: chr4: 12,113,443:121,140,06. The amplicons were sequenced on a high-throughput sequencing platform (Wide-Seq), and the data were analyzed using Bismark software. The boxplot represents the range of the percentage of DNA methylation at various CpG sites in each target region. The median methylation at both targets is higher in KD cells compared with VC cells. p values were calculated using Wilcoxon matched-pairs rank test: *$p < 0.05$; **$p < 0.01$; ***$p < 0.005$.

VC, vector control; KD, shRNA-mediated knockdown of *Dnmt3bas*; OE, overexpression of *Dnmt3bas*; spl, spliced *Dnmt3bas*; uns, unspliced *Dnmt3bas*; F3, exon 2 fragment of *Dnmt3bas*.

of *Dnmt3bas* compared with VC cells (Figure 2D). Furthermore, cell fractionation analysis of the *Dnmt3bas* KD and OE cells showed a proportional change in the *Dnmt3bas* transcript level in the cytoplasm and nucleus (Figure S2H), supporting the localization of *Dnmt3bas* primarily in the nucleus. We also ruled out the potential confounding impact of impaired pluripotency in the *Dnmt3bas*-manipulated cell lines. Cell morphology and gene expression analysis pre- and post-differentiation show no significant difference between the three cell lines (Figures S2I and S2J). In UD and day 6 differentiated VC, KD, and OE cell lines, no difference in *Dnmt3b* basal expression was observed (Figure 2E). However, compared with VC cells, which showed a 15-fold induction of *Dnmt3b* at D3, the induction of *Dnmt3b* in the KD cells increased to nearly 30-fold. A similar effect on *Dnmt3b* expression was observed in both KD1 and KD2 cells (Figure S2K); therefore, only KD1 cells were used for further investigation. Interestingly, OE of *Dnmt3bas* showed an opposite effect on *Dnmt3b* induction with only a 7-fold increase in *Dnmt3b* expression on day 3 post-differentiation in the OE cells. The repressive activity of *Dnmt3bas* was specific for only the spliced isoform since cells overexpressing the unspliced *Dnmt3bas* behaved similarly to VC cells (Figure 2E). In addition, *Dnmt3b* induction in KD cells was rescued to a lower level by OE of only the spliced isoform of *Dnmt3bas* and not by the unspliced and truncated shRNA-resistant *Dnmt3bas* fragment (Figures 2F and 2G). These data confirm the *trans* activity of the spliced *Dnmt3bas* transcript.

To test whether *Dnmt3bas* modulated the kinetics, magnitude, or both of *Dnmt3b* induction, we measured *Dnmt3b* transcript levels every 24 h post-differentiation. The data were fit to a non-linear regression using GraphPad Prism. Whereas an apparent change in the magnitude of induction was recorded, it peaked at the same time point in all three cell lines, indicating the effect of *Dnmt3bas* on the magnitude of *Dnmt3b* induction (Figure 2H).

We next asked if alternative splicing of *Dnmt3b* was affected in *Dnmt3bas* KD and OE cell lines. *The* ratio of *Dnmt3b1:Dnmt3b6* was determined using RT-PCR analysis in VC, KD, and OE cells cultured in the 2i medium (Figure 2I). The *Dnmt3b1*:*Dnmt3b6* ratio in VC cells pre- and post-differentiation was similar to the wild-type (WT) 2i-ESCs shown in Figure 1B. *Dnmt3b6* is the predominant isoform in UD 2i-ESCs. Post differentiation (day 3) transcriptional induction of Dnmt3b was accompanied by increased exon inclusion, thus transcribing *Dnmt3b1* as a major isoform. Although this trend was prevalent in KD and OE cells, we observed a peculiar increase in the *Dnmt3b1*:*Dnmt3b6* ratio in OE cells post-differentiation. These data, collectively, suggest that the repressive effect of *Dnmt3bas* maintains the *Dnmt3b* promoter/proximal enhancer in the primed state in UD cells and fine-tunes the magnitude of *Dnmt3b* induction and alternative splicing in response to differentiation signals.

The potential impact of *Dnmt3bas* manipulations on genomic methylation was tested using methylation-sensitive restriction, which showed a delay in the gain of methylation in both KD and OE cells compared with VC cells (Figure S2L). Bisulfite sequencing of two Dnmt3b-specific target regions showed a significant increase in DNA methylation in KD cells compared with the VC and OE cells on day 2 post-differentiation[60] (Figure 2J). However, on day 4, DNA methylation differences between various cell lines were less significant (Figure S2M). In the context of VC, KD, and OE cell lines, if there are differences in the initially established methylation patterns due to altered expression of DNMT3B, the maintenance activity of DNMT1 can potentially act to close those differences. DNMT1 would recognize and methylate hemi-methylated sites during DNA replication, thereby restoring or equalizing the methylation patterns across the different cell lines.[61]

Dnmt3bas modulates the chromatin modification state at Dnmt3b regulatory regions

To understand the mechanism of *Dnmt3bas* in regulating *Dnmt3b* induction, we measured chromatin modifications, i.e., H3K4me1, H3K27me3, and H3K27Ac, at *Dnmt3b* regulatory regions during differentiation and compared changes in KD and OE cells with VC cells. In all three cell lines, an increase in H3K4me1 was observed at both proximal and distal enhancer regions at day 3 post-differentiation compared with the UD cells (Figure 3A). Loss of H3K27me3 was accompanied by the gain of H3K27Ac at the proximal and distal enhancer region in day 3 cells (Figures 3B and 3C). Similar changes in H3K27me3 and H3K27Ac were observed at the CGI region of the Dnmt3b promoter (Figures 3D and 3E). However, at the proximal enhancer and the CGI region, we observed a lower and a higher enrichment of H3K27me3 in UD KD and OE cells, respectively, compared with the VC cells (Figures 3D and S3A). An opposite trend in H3K27Ac was observed at the Dnmt3b promoter CGI in these cells (Figure 3E), corresponding to the difference in Dnmt3b induction in these cell lines. No difference in DNA methylation at promoter and enhancer regions was observed between the VC, KD, and OE cell lines (Figures S3B and S3C).

Based on the above data, we speculated that *Dnmt3bas* recruits the PRC2 complex to *Dnmt3b cis*-regulatory regions, similar to several other lncRNAs known to escort the PRC2 complex to their target sites.[29,50] The presence of the PRC2 complex was confirmed by SUZ12 chromatin immunoprecipitation (ChIP), which shows strong enrichment at the Dnmt3b promoter. In alignment with H3K27me3, significantly lower and higher SUZ12 enrichment was observed in the KD and OE cells, respectively, compared with VC cells (Figure 3F). We showed the direct interaction of *Dnmt3bas* with the PRC2 complex by RNA pull-down assay using *in-vitro*-transcribed biotinylated *Dnmt3bas* (Figure 3G). Sequence analysis of *Dnmt3bas* using the G-quad analysis tool (GQRS mapper, key resource table) showed several potential G-quadruplex structures. K+, not Li+, ions stabilize the G-quad structure[62] and promote PRC2 binding. Western blot shows a strong interaction of *Dnmt3bas* with AEBP2 and SUZ12 in the KCl buffer. However, AEBP2 binding was reduced in the presence of LiCl buffer, suggesting a direct interaction of this subunit to the *Dnmt3bas* G-quad structure. In contrast, the binding of the splicing factor hnRNPK was unaffected by different buffer conditions.[63]

These data demonstrate that *Dnmt3bas* recruits PRC2 at the *Dnmt3b* promoter/proximal enhancer (PE) region maintained at basal activity and thus fine-tunes the gain of H3K27Ac and *Dnmt3b* induction post-differentiation.

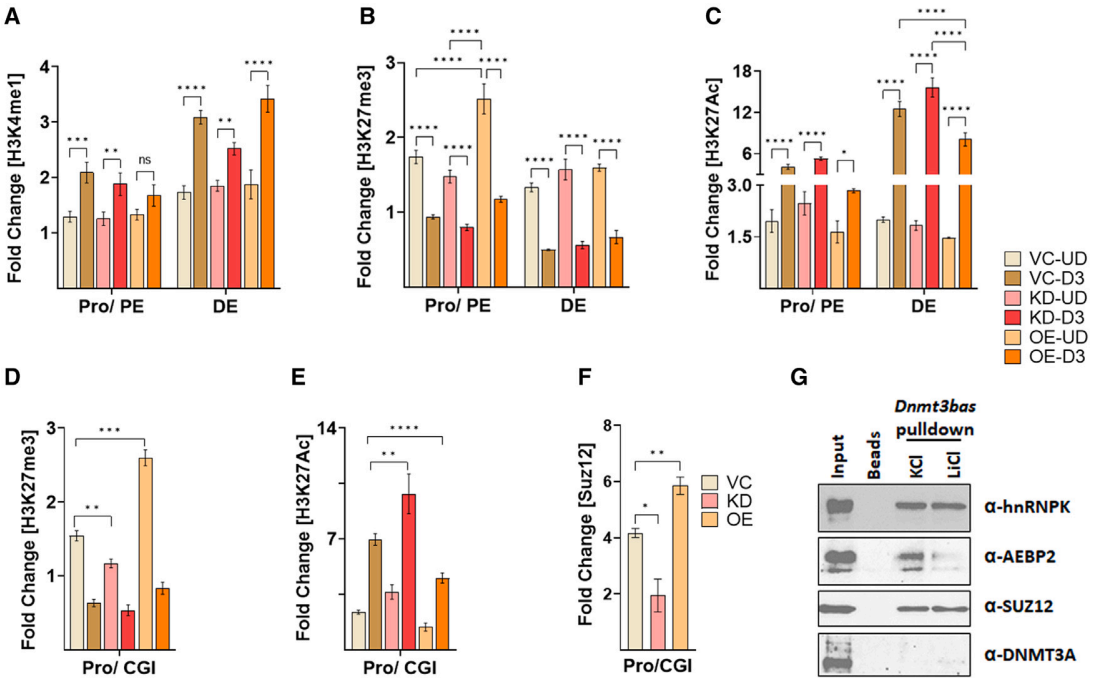

Figure 3. Chromatin modification at Dnmt3b regulatory elements in *Dnmt3bas*-manipulated ESCs

(A–E) ChIP-qPCR assays show fold enrichment over input normalized to control. Histone modifications at Dnmt3b regulatory elements (A) H3K4me1, (B and D) H3K27me3, and (C and E) H3K27Ac pre- and D3 post-differentiation in VC, KD, and OE cells.

(G) Fold enrichment of the PRC2 complex component SUZ12 at the *Dnmt3b* promoter CGI region. p values were derived from ANOVA test: *$p < 0.05$; **$p < 0.01$; ***$p < 0.005$. Results are presented as normalized mean values ± SEM. See also Figure S3.

(H) Western blot analysis of *Dnmt3bas*-interacting proteins from the RNA pull-down assays performed in 100 mM KCl- or 100 mM LiCl-containing buffer. Dnmt3a is used as a negative control and hnRNPK as a positive control for RNA binding.

Abbreviations are as described in the legend of Figures 1 and 2.

Dnmt3bas is localized at the Dnmt3b promoter and affects E-P looping

We performed a 3C assay in VC, KD, and OE cell lines to test the effect of *Dnmt3bas* on distal E-P interaction. The data show little or no effect on the interaction frequency of *Dnmt3b* distal enhancer and promoter in the UD 2i-ESCs (Figure 4A). Given the proximity of enhancer and promoter in the UD state, the crosslinking method used for the 3C assays poses a challenge to determine a significant increase in the interaction post-differentiation. However, corresponding to higher transcriptional induction, we observed a small but significant increase in the E-P interaction frequency in KD cells compared with the VC cells (Figure 4B).

To test if *Dnmt3bas* RNA is associated with the distal enhancer chromatin, we performed the chromatin isolation by RNA purification (ChIRP) assay in WT and transgenic (VC, OE, and KD) 2i-ESCs pre- and post-differentiation. Using probes specific to exon or intron regions of *Dnmt3bas*, RNA recovery analysis showed high and specific recovery of the spliced *Dnmt3bas* from the RNA fraction of UD and day 3 differentiated cells (Figures 4C and S4). From the DNA fraction, approximately 10-fold higher enrichment of the *Dnmt3b* promoter region was measured compared with the distal enhancer (Figure 4D). A significantly lower and higher enrichment of the Dnmt3b promoter region was observed in KD and OE cells, respectively, compared with VC cells, and no significant change was observed in the enrichment of the Dnmt3b distal enhancer region (Figure 4E). These data confirm that spliced *Dnmt3bas* is localized primarily at the *Dnmt3b* promoter.

hnRNPL binds *Dnmt3bas* and regulates Dnmt3b alternative splicing

To determine the mechanism by which *Dnmt3bas* regulates the alternative splicing of *Dnmt3b*, we performed an RNA pull-down assay using *in-vitro*-transcribed biotinylated *Dnmt3bas* and control *as-Dnmt3bas* RNAs to identify *Dnmt3bas*-interacting proteins (Figure 5A). On a Coomassie-stained SDS-PAGE, a distinct protein band at around 60 kDa was explicitly observed in the *Dnmt3bas* elution and was absent in the control sample (Figure S5A). Mass spectrometry (MS) analysis of proteins in the excised fragment from control and experimental lanes showed a strong enrichment of hnRNPL in the experimental sample. The protein band was confirmed to be hnRNPL by immunoblotting the RNA pull-down samples (Figure 5B). To examine the *in vivo* interaction of hnRNPL with *Dnmt3bas*, we performed a western blot analysis of the protein fraction from the *Dnmt3bas* ChIRP assay. The data showed a strong signal of hnRNPL in the experimental sample that was absent in the RNase-treated control sample (Figure 5C). ChIP assay using an anti-hnRNPL antibody showed significant and specific enrichment of hnRNPL

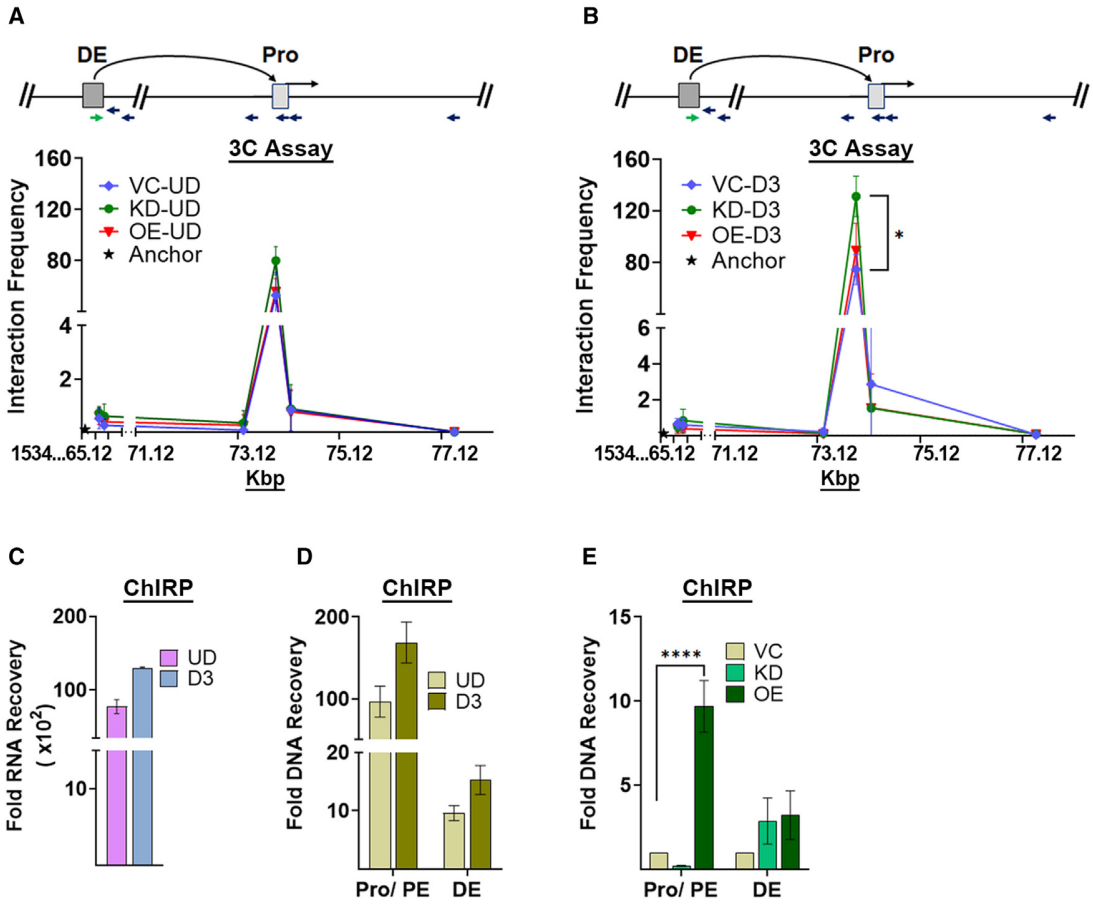

Figure 4. *Dnmt3bas* associates with Dnmt3b enhancers and influences E-P looping

(A and B) Chromatin interaction assay, 3C, shows an interaction of the DE with the promoter of Dnmt3b. 3C assays were performed in undifferentiated and day 3 differentiated VC, KD, and OE cells. Primer positions were as described in the legend of Figure 1, and primer at DE was used as bait.

(C and D) ChIRP (chromatin isolation by RNA purification) was performed using *Dnmt3bas*-specific biotinylated probes. The RNA and DNA fractions from the eluate were separated and used to probe for (C) *Dnmt3bas* transcript and (D) Dnmt3b Pro/PE and DE regions, respectively.

(E) Fold DNA recovery of Pro/PE and DE regions in *Dnmt3bas* KD and OE cells compared with that in the VC cells. Results are presented as normalized mean values ± SEM. p values were derived from Student's t test: *$p < 0.05$; ****$p < 0.0001$. See also Figure S4.

Abbreviations as described in Figures 1 and 2 legends.

at the *Dnmt3b* promoter, confirming its *in vivo* binding at these sites (Figure 5D).

hnRNPL binds CA repeats with high affinity,[64] and *Dnmt3bas* contains two clusters of CA repeats within exon 2 spaced apart by about 50 bp. To locate the hnRNPL-binding sites, we performed RNA pull-down assays using *Dnmt3bas* fragments (Figure 5E). Compared to a weak binding with the exon 1 fragment (F1), strong hnRNPL binding was observed with the intermediate and the exon 2 RNA fragments (F2 and F3) containing both CA clusters (Figure 5F). Next, we systematically mutated the CA clusters in the full-length *Dnmt3bas* and used the variants for the RNA pull-down assay. Variant 1 has mutations in only cluster 2, and variants 2 and 3 have different mutations in clusters 1 and 2. Whereas the hnRNPL binding of variant 1 is similar to that of WT *Dnmt3bas*, the binding to variants 2 and 3 was strongly reduced (Figure 5G), indicating that hnRNPL predominantly binds to the cluster 1 site. Thus, we conclude that hnRNPL specifically binds *Dnmt3bas* and is recruited to the *Dnmt3b* promoter region.

Previous studies have shown that the RNA-binding protein hnRNPL regulates alternative splicing (AS).[65–67] Based on the observation that the ratio of *Dnmt3b1*:*Dnmt3b6* increased in *Dnmt3bas* OE cells post-differentiation, we asked if increased exon inclusion was due to higher hnRNPL recruitment by *Dnmt3bas*. Therefore, we overexpressed *Dnmt3bas* variants with mutations in hnRNPL-binding sites in 2i-ESCs. Transgenic cell lines were differentiated, and alternative splicing of *Dnmt3b* was analyzed at day 3 post-differentiation. Compared with cells overexpressing WT *Dnmt3bas*, the ratio of *Dnmt3b1*:*Dnmt3b6* in cells overexpressing variants was similar to that in the VC cells (Figure 5H). Furthermore, small interfering RNA (siRNA)-mediated depletion of hnRNPL in *Dnmt3bas* OE cells rescued the *Dnmt3b6*:*Dnmt3b1* ratio to that in VC cells (Figures 5I and S5B), suggesting that increased recruitment of hnRNPL at the

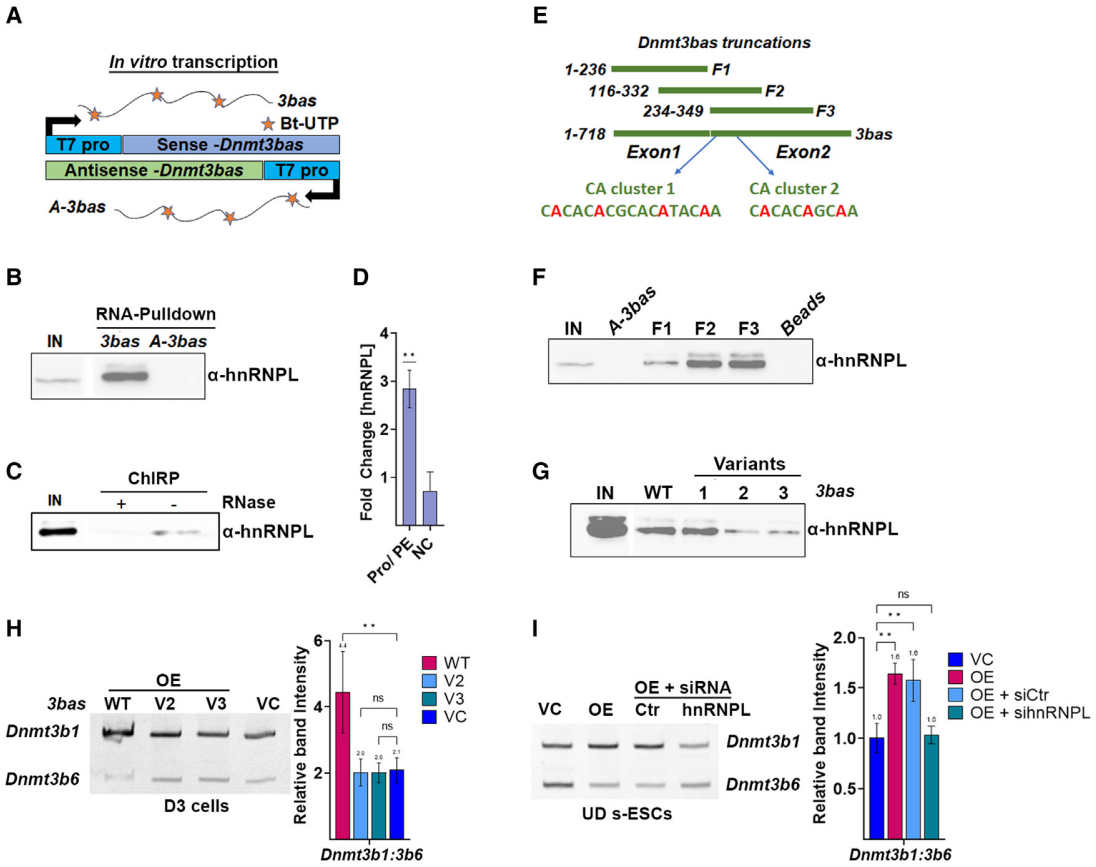

Figure 5. hnRNPL binds to a CA-repeat region of *Dnmt3bas* and regulates *Dnmt3b* alternative splicing

(A and E) Schematic showing the experimental design for *in vitro* transcription of (A) *Dnmt3bas*, antisense control transcript, and (E) *Dnmt3bas* fragments used for RNA pull-down assays. The *in vitro* transcription was performed using biotinylated UTP and nuclear extract from 2i-ESCs.

(B, C, F, and G) Western blot analysis of hnRNPL after RNA pull-down assay using (B) sense and antisense *Dnmt3bas* transcripts, (F) truncated fragments of *Dnmt3bas* transcript, and (G) variants of *Dnmt3bas* with substitutions in hnRNPL-binding sites.

(C) Western blot analysis of hnRNPL in the protein fraction from ChIRP assay in RNAse-treated and untreated samples.

(D) ChIP-qPCR assays show fold enrichment over the input of hnRNPL. NC is the control region in the mouse genome. p values were derived from the Student's t test: *$p < 0.05$; **$p < 0.01$.

(H and I) Ratio of *Dnmt3b1*/*Dnmt3b6* isoforms at day 3 post differentiation (H) from cells OE wild type and V2 and V3 variants of *Dnmt3bas* and (I) from *Dnmt3bas* OE serum cultured cells treated with siRNA to knock down hnRNPL. The bar graphs show the ratio of quantified band intensity from at least 3 gels. Results are presented as normalized mean values ± SEM. $n \geq 3$. p values were derived from the ANOVA test: *$p < 0.05$; **$p < 0.01$. See also Figure S5.

3bas, *Dnmt3bas* transcript; A-3bas, antisense of *Dnmt3bas* transcript; bt-UTP, biotinylated UTP; IN, input; NC, negative control; cluster 1 and cluster 2, predicted hnRNPL-binding sites on *Dnmt3bas*; V1, V2, and V3, red font shows the sites of substitutions in variants of *Dnmt3bas* in cluster 2 (V1) and clusters 1 and 2 (V2 and V3). Other abbreviations refer to the legends of Figures 1 and 2.

Dnmt3b promoter increases the number of exon inclusion events.

Given that *Dnmt3bas* recruits hnRNPL to the *Dnmt3b* promoter, we speculate that post-induction, the *Dnmt3bas*-hnRNPL complex facilitates the interaction of hnRNPL with elongating RNA Pol II, which ferries hnRNPL to alternatively spliced sites at the 3′ end of the *Dnmt3b* transcript. This model is supported by recent studies showing that the interaction of SETD2 with hnRNPL and elongating RNA Pol II couples transcriptional elongation and alternative splicing.[68–70] We observed no significant change in the deposition of H3K36me3 at the 3′ end of the *Dnmt3b* gene in *Dnmt3bas* OE cells compared with the VC cells (Figure S5C), confirming that the activities of SETD2 and hnRNPL are not dependent on their interaction with each other.[70] However, this observation does not exclude the potential role of SETD2 in mediating the interaction of hnRNPL with elongating RNA Pol II.

A mechanistic model of Dnmt3bas

Our study comprehensively examined the mechanism that regulates the spatiotemporal expression of *Dnmt3b* during early development (Figure 6). The data revealed the unique role of *Dnmt3bas* in transcriptional priming and the coordination of transcriptional induction and alternative splicing of *Dnmt3b*. This role of *Dnmt3bas* is mediated by its interaction with the PRC2 complex and the splicing protein hnRNPL. In the UD 2i-ESCs, *Dnmt3b* is expressed at the basal level, and *Dnmt3bas* maintains the *Dnmt3b* promoter

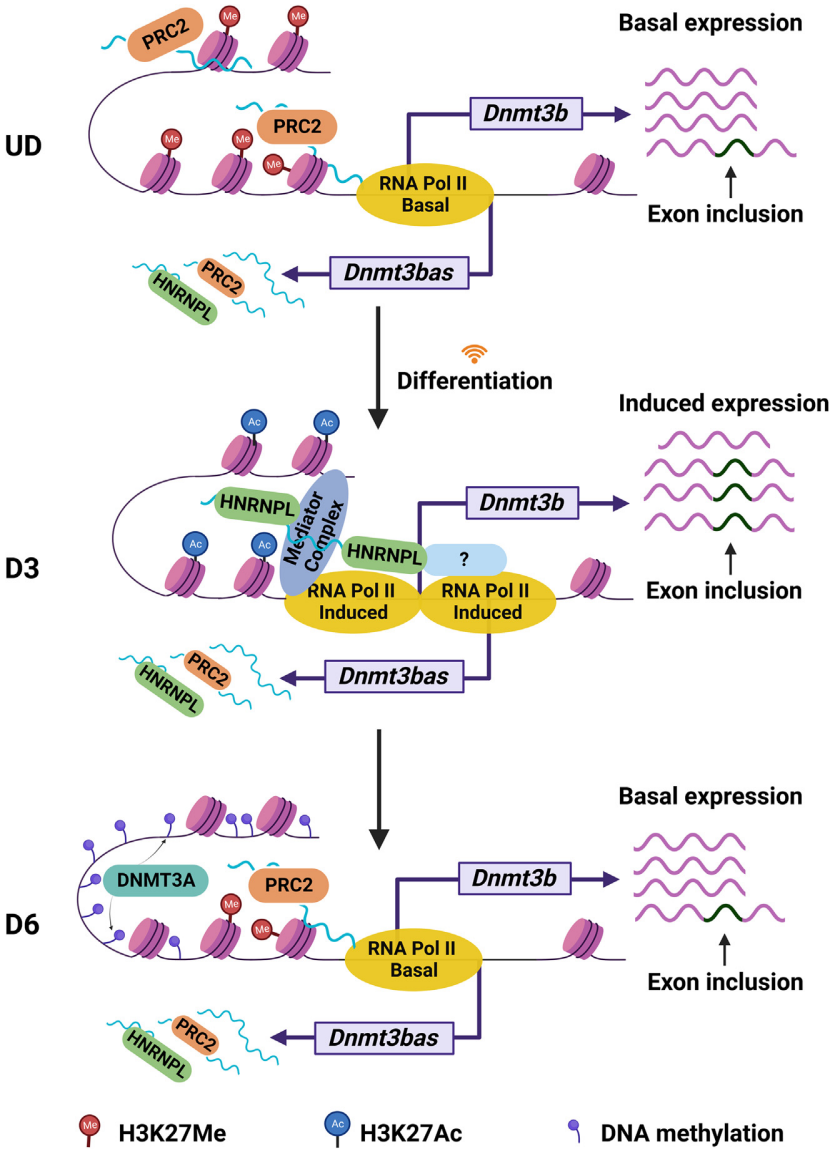

Figure 6. Model of epigenetic changes at pluripotency gene enhancers during stem cell differentiation

In the undifferentiated (UD) state, *Dnmt3bas* targets the PRC2 complex, which adds H3K27me3 at Dnmt3b regulatory elements. Under basal expression, the *Dnmt3b* transcript predominantly undergoes exon exclusion of exons 23 and 24 (*Dnmt3b6* isform). In response to differentiation signals (day 3), *Dnmt3b* expression is induced with a concerted switch in alternative splicing to exon inclusion (*Dnmt3b1* isoform). *Dnmt3bas* recruits the splicing factor hnRNPL to the transcriptionally active *Dnmt3b* promoter. Once at the promoter, hnRNPL hitchhikes RNA Pol II, potentially through an adaptor protein, and is delivered to *Dnmt3b* splice sites. Post-differentiation (day 6), DNA methylation by DNMT3A appears at the promoter-proximal and -distal enhancers, and not at the CGI promoter of *Dnmt3b*, maintaining the basal expression of *Dnmt3b6*. In particular, the CGI promoter regains H3K27me3, suggesting the role of a lower but persistent expression of *Dnmt3bas* in stabilizing the activity of the PRC2 complex at the CGI promoter.

in a primed state by targeting PRC2 activity. When differentiation is triggered, *Dnmt3b* expression is induced by enhancement of E-P interaction and deposition of H3K27Ac. Higher expression of *Dnmt3b* is also accompanied by increased exon inclusion and switching of alternative splicing in favor of *Dnmt3b1* transcription. *Dnmt3bas* facilitates this alternative splicing switch by delivering the splicing factor hnRNPL at the transcriptionally active *Dnmt3b* promoter. *Dnmt3bas* bridges the interaction of hnRNPL with elongating RNA Pol II, ensuring its delivery to alternative splice sites. Following induction, the post-differentiation repression of *Dnmt3b* is mediated by DNA methylation at proximal and distal enhancers. Notably, the CGI promoter regains the H3K27me3 mark, suggesting the role of a lower but persistent expression of *Dnmt3bas*, which is essential for stabilizing the activity of the PRC2 complex at the CGI promoter.

DISCUSSION

The spatiotemporal regulation of *Dnmt3b* expression is critical for development and cellular homeostasis. An aberrant increase in *DNMT3B* expression leads to DNA hypermethylation and loss of gene regulation in various human diseases.[71–73] Here, we used naive ESC differentiation as an early developmental model to report *Dnmt3bas*/*Dnmt3b* as a coordinately expressed gene pair where the lncRNA *Dnmt3bas* regulates transcriptional induction and alternative splicing of *Dnmt3b* mRNA.

Role of Dnmt3bas in Dnmt3b transcriptional induction

During 2i medium adaptation and ESC differentiation, *Dnmt3bas* expression is lowest when the *Dnmt3b* gene is expressed at high levels, suggesting a potential transcriptional interference mechanism.[74] Nevertheless, post-differentiation repression of *Dnmt3b* did not stimulate *Dnmt3bas* expression, suggesting a distinct regulatory mechanism that controls *Dnmt3bas* expression. Given that *Dnmt3bas* is expressed within the promoter of the *Dnmt3b* gene, genetic manipulations using CRISPR-Cas9 could not be employed. However, we observed a significant effect of *Dnmt3bas* on *Dnmt3b* expression by using shRNA-mediated KD and OE of *Dnmt3bas* RNA in the 2i-ESCs. In response to the differentiation signal, a concomitant loss of H3K27me3 precedes the gain of H3K27Ac to activate *Dnmt3b* enhancers, which engage strongly with the promoter (E-P loop) to facilitate transcriptional induction. Some lncRNAs can help stabilize the E-P loop by interacting with components of the Mediator

complex like Med1 and Med12[26] or cooperate with CTCF-mediated chromatin interactions to affect the transcription of genes.[75–77] However, we show that *Dnmt3bas* interacts with the PRC2 complex, and this interaction could be further potentiated by hnRNPK binding.[63] In *Dnmt3bas* KD cells, we observed an increase in the E-P interaction and H3K27Ac at the distal enhancer, suggesting the role of *Dnmt3bas* in stabilizing repressive PRC2 complex binding. Furthermore, the proximity of the distal enhancer to the Dnmt3b promoter in UD cells implies a dual role of the E-P loop: (1) facilitating the recruitment of PRC2 complex to the distal enhancer and (2) mediating a quick transcriptional response to the differentiation signal.

Interestingly, neither the expression of *Dnmt3bas* nor the enrichment of H3K27me3 at distal regulatory elements increased during the post-differentiation repression of *Dnmt3b*. Instead, we observed a loss of H3K27Ac and a gain of DNA methylation in regions further upstream, flanking the 5′ end of the *Dnmt3b* promoter CGI. However, at the CGI, which is maintained in an unmethylated state, we observed an increase in H3K27me3, suggesting the role of the PRC2 complex in maintaining the *Dnmt3b* promoter in a repressed state post-differentiation. This observation also suggests that low but significant expression of *Dnmt3bas* post-differentiation could mediate the maintenance of H3K27me3 at the CGI.

Role of Dnmt3bas in Dnmt3b alternative splicing

Here, we show that 2i-cultured ESCs, a homogeneous population of cells in the ground state of pluripotency, express low levels of *Dnmt3b* and the short catalytically inactive *Dnmt3b6* as the major isoform. Our data suggest that in 2i-ESCs, whereas the basal transcription of *Dnmt3b6* retains the Dnmt3b promoter in a primed state, the promoter activation process appends a mechanism that facilitates exon inclusion to generate the full-length transcript, *Dnmt3b1*. Therefore, besides temporal regulation of *Dnmt3b* transcription, this observation signifies the role of *Dnmt3b* alternative splicing in genome-wide loss of DNA methylation in 2i-ESCs and *de novo* DNA methylation during early development.

Our data showed hnRNPL among several unique *Dnmt3bas*-binding proteins. Functional characterization of *Dnmt3bas*/hnRNPL interaction showed its role in inducible exon inclusion, a process critical for expressing catalytically active Dnmt3b1 during differentiation. hnRNPL is a known regulator of alternative splicing,[65–67] RNA stability,[78] and transcriptional regulation in partnership with multiple lncRNAs.[79–81] Previous studies have shown that the binding of hnRNPs, including hnRNPK, hnRNPU, and U1 small nuclear ribonucleoprotein (snRNP) binding, facilitate chromatin tethering and nuclear retention of lncRNAs.[82–85] Med23 was also shown to recruit hnRNPL to the promoter of genes, a role similar to *Dnmt3bas*.[86] These observations suggest that the nucleoprotein constitution at gene promoters can determine both transcription and splicing outcomes.[87]

Implications of Dnmt3bas-hnRNPL interaction

Recent studies have shown the interaction of SETD2 with hnRNPL and proposed that SETD2 hitchhikes to the elongating RNA Pol II and transports hnRNPL to the splice sites as they emerge during chain elongation.[68–70] Our study suggests that the recruitment of hnRNPL by *Dnmt3bas* to the promoter of *Dnmt3b* facilitates hnRNPL-SETD2 transfer. Given that the RNA-binding domain of hnRNPL, RRM2, also interacts with SETD2, the interaction of hnRNPL with SETD2 and *Dnmt3bas* could be mutually exclusive. This prediction is supported by the absence of SETD2 in the RNA pull-down/MS analysis of *Dnmt3bas*-binding proteins. Therefore, interaction choice could be dictated by the proximity and binding strength of the RRM2 with RNA versus SETD2.

Based on the expression pattern of *Dnmt3bas*, it could reconstitute various nucleoprotein complexes ubiquitously. However, the mechanism most consistent with the published data so far that explains the specific activity of the *Dnmt3bas*/hnRNPL complex during transcriptional induction is that in the induced state, a bulk increase in elongating RNA Pol II at the Dnmt3b promoter allows interaction with the SETD2/RNA Pol II elongation complex, which ferries hnRNPL to the alternative splice sites in the gene body. A dramatic increase in H3K36me3 in the Dnmt3b gene body and at the 3′ end on day 3 post-differentiation indicates increased SETD2 activity post-induction (Figure S5C).

Furthermore, in contrast to hnRNPL, hnRNPI (PTBP1) is involved in the exon exclusion in the *Dnmt3b* mRNA,[88] suggesting that their antagonistic activity determines the splice site choice in *Dnmt3b* pre-mRNA. Both proteins bind to similar polypyrimidine tracts (CA repeats) on RNA through their RRM domains and interact with each other.[89] However, the mechanism by which their antagonistic activity at alternative splice sites is regulated is unknown. It would be interesting to determine the mechanism of potential cross-talk between antagonist splice factors and chromatin modifiers that fine-tunes the relative levels of the alternatively spliced isoforms in response to varying physiological conditions.

STAR★METHODS

Detailed methods are provided in the online version of this paper and include the following:

- KEY RESOURCES TABLE
- RESOURCE AVAILABILITY
  - Lead contact
  - Materials availability
  - Data and code availability
- EXPERIMENTAL MODEL AND STUDY PARTICIPANT DETAILS
- METHOD DETAILS
  - Cell culture and transgenic cell lines
  - Microscopy
  - RT-qPCR and RT-PCR
  - Chromosome conformation capture assay (3C)
  - RNA-pulldown and hnRNPL binding assays
  - Subcellular fractionation
  - Chromatin isolation by RNA purification (ChIRP)
  - DNA methylation analysis
  - Chromatin immunoprecipitation
  - Western blot
  - RNA-Fluorescent in-situ hybridization assay (RNA-FISH)

- In-gel trypsin digestion and mass spectrometry
- QUANTIFICATION AND STATISTICAL ANALYSIS

SUPPLEMENTAL INFORMATION

Supplemental information can be found online at https://doi.org/10.1016/j.celrep.2023.112587.

ACKNOWLEDGMENTS

We are thankful to Gowher lab members for their discussions. This work was supported by NSF award 1716678 and NIH R01 GM118654-01. In addition, we thank Dr. Tiaping Chen for *Dnmt3a*$^{-/-}$ ESCs. Finally, the authors gratefully acknowledge the Walter Cancer Foundation, DNA Sequencing Facility, and support from the Purdue University Center for Cancer Research, P30CA023168.

AUTHOR CONTRIBUTIONS

M.S.D., I.K.M., M.H., S.M., I.S.S., M.C.H., H.C.W., N.E.B., M.C., M.L.E., and H.J.T. performed the experiments. M.C.H. and H.G. analyzed the MS data. M.S.D., I.K.M., and H.G. wrote the manuscript.

DECLARATION OF INTERESTS

The authors declare no competing interests.

INCLUSION AND DIVERSITY

We support inclusive, diverse, and equitable conduct of research.

Received: June 3, 2022
Revised: March 16, 2023
Accepted: May 16, 2023

REFERENCES

1. Greenberg, M.V.C., and Bourc'his, D. (2019). The diverse roles of DNA methylation in mammalian development and disease. Nat. Rev. Mol. Cell Biol. *20*, 590–607. https://doi.org/10.1038/s41580-019-0159-6.
2. Okano, M., Bell, D.W., Haber, D.A., and Li, E. (1999). DNA methyltransferases Dnmt3a and Dnmt3b are essential for de novo methylation and mammalian development. Cell *99*, 247–257. https://doi.org/10.1016/s0092-8674(00)81656-6.
3. Okano, M., Xie, S., and Li, E. (1998). Cloning and characterization of a family of novel mammalian DNA (cytosine-5) methyltransferases. Nat. Genet. *19*, 219–220. https://doi.org/10.1038/890.
4. Gopalakrishnan, S., Sullivan, B.A., Trazzi, S., Della Valle, G., and Robertson, K.D. (2009). DNMT3B interacts with constitutive centromere protein CENP-C to modulate DNA methylation and the histone code at centromeric regions. Hum. Mol. Genet. *18*, 3178–3193. https://doi.org/10.1093/hmg/ddp256.
5. Norvil, A.B., AlAbdi, L., Liu, B., Tu, Y.H., Forstoffer, N.E., Michie, A.R., Chen, T., and Gowher, H. (2020). The acute myeloid leukemia variant DNMT3A Arg882His is a DNMT3B-like enzyme. Nucleic Acids Res. *48*, 3761–3775. https://doi.org/10.1093/nar/gkaa139.
6. Watanabe, D., Suetake, I., Tada, T., and Tajima, S. (2002). Stage- and cell-specific expression of Dnmt3a and Dnmt3b during embryogenesis. Mech. Dev. *118*, 187–190. https://doi.org/10.1016/s0925-4773(02)00242-3.
7. Hirasawa, R., and Sasaki, H. (2009). Dynamic transition of Dnmt3b expression in mouse pre- and early post-implantation embryos. Gene Expr. Patterns *9*, 27–30. https://doi.org/10.1016/j.gep.2008.09.002.
8. Ficz, G., Hore, T.A., Santos, F., Lee, H.J., Dean, W., Arand, J., Krueger, F., Oxley, D., Paul, Y.L., Walter, J., et al. (2013). FGF signaling inhibition in ESCs drives rapid genome-wide demethylation to the epigenetic ground state of pluripotency. Cell Stem Cell *13*, 351–359. https://doi.org/10.1016/j.stem.2013.06.004.
9. Leitch, H.G., McEwen, K.R., Turp, A., Encheva, V., Carroll, T., Grabole, N., Mansfield, W., Nashun, B., Knezovich, J.G., Smith, A., et al. (2013). Naive pluripotency is associated with global DNA hypomethylation. Nat. Struct. Mol. Biol. *20*, 311–316. https://doi.org/10.1038/nsmb.2510.
10. Ying, Q.L., Wray, J., Nichols, J., Batlle-Morera, L., Doble, B., Woodgett, J., Cohen, P., and Smith, A. (2008). The ground state of embryonic stem cell self-renewal. Nature *453*, 519–523. https://doi.org/10.1038/nature06968.
11. Xie, S., Wang, Z., Okano, M., Nogami, M., Li, Y., He, W.W., Okumura, K., and Li, E. (1999). Cloning, expression and chromosome locations of the human DNMT3 gene family. Gene *236*, 87–95. https://doi.org/10.1016/s0378-1119(99)00252-8.
12. Ostler, K.R., Davis, E.M., Payne, S.L., Gosalia, B.B., Expósito-Céspedes, J., Le Beau, M.M., and Godley, L.A. (2007). Cancer cells express aberrant DNMT3B transcripts encoding truncated proteins. Oncogene *26*, 5553–5563. https://doi.org/10.1038/sj.onc.1210351.
13. Saito, Y., Kanai, Y., Sakamoto, M., Saito, H., Ishii, H., and Hirohashi, S. (2002). Overexpression of a splice variant of DNA methyltransferase 3b, DNMT3b4, associated with DNA hypomethylation on pericentromeric satellite regions during human hepatocarcinogenesis. Proc. Natl. Acad. Sci. USA *99*, 10060–10065. https://doi.org/10.1073/pnas.152121799.
14. Weisenberger, D.J., Velicescu, M., Cheng, J.C., Gonzales, F.A., Liang, G., and Jones, P.A. (2004). Role of the DNA methyltransferase variant DNMT3b3 in DNA methylation. Mol. Cancer Res. *2*, 62–72.
15. Wang, J., Bhutani, M., Pathak, A.K., Lang, W., Ren, H., Jelinek, J., He, R., Shen, L., Issa, J.P., and Mao, L. (2007). Delta DNMT3B variants regulate DNA methylation in a promoter-specific manner. Cancer Res. *67*, 10647–10652. https://doi.org/10.1158/0008-5472.CAN-07-1337.
16. Duymich, C.E., Charlet, J., Yang, X., Jones, P.A., and Liang, G. (2016). DNMT3B isoforms without catalytic activity stimulate gene body methylation as accessory proteins in somatic cells. Nat. Commun. *7*, 11453. https://doi.org/10.1038/ncomms11453.
17. Zeng, Y., Ren, R., Kaur, G., Hardikar, S., Ying, Z., Babcock, L., Gupta, E., Zhang, X., Chen, T., and Cheng, X. (2020). The inactive Dnmt3b3 isoform preferentially enhances Dnmt3b-mediated DNA methylation. Genes Dev. *34*, 1546–1558. https://doi.org/10.1101/gad.341925.120.
18. Guil, S., and Esteller, M. (2009). DNA methylomes, histone codes and miRNAs: tying it all together. Int. J. Biochem. Cell Biol. *41*, 87–95. https://doi.org/10.1016/j.biocel.2008.09.005.
19. Szyf, M. (2005). Therapeutic implications of DNA methylation. Future Oncol. *1*, 125–135. https://doi.org/10.1517/14796694.1.1.125.
20. Kulis, M., and Esteller, M. (2010). DNA methylation and cancer. Adv. Genet. *70*, 27–56. https://doi.org/10.1016/B978-0-12-380866-0.60002-2.
21. Mensah, I.K., Norvil, A.B., AlAbdi, L., McGovern, S., Petell, C.J., He, M., and Gowher, H. (2021). Misregulation of the expression and activity of DNA methyltransferases in cancer. NAR Cancer *3*, zcab045. https://doi.org/10.1093/narcan/zcab045.
22. Huntriss, J., Hinkins, M., Oliver, B., Harris, S.E., Beazley, J.C., Rutherford, A.J., Gosden, R.G., Lanzendorf, S.E., and Picton, H.M. (2004). Expression of mRNAs for DNA methyltransferases and methyl-CpG-binding proteins in the human female germ line, preimplantation embryos, and embryonic stem cells. Mol. Reprod. Dev. *67*, 323–336. https://doi.org/10.1002/mrd.20030.
23. Rinn, J.L., Kertesz, M., Wang, J.K., Squazzo, S.L., Xu, X., Brugmann, S.A., Goodnough, L.H., Helms, J.A., Farnham, P.J., Segal, E., and Chang, H.Y. (2007). Functional demarcation of active and silent chromatin domains in human HOX loci by noncoding RNAs. Cell *129*, 1311–1323. https://doi.org/10.1016/j.cell.2007.05.022.
24. Thakur, N., Tiwari, V.K., Thomassin, H., Pandey, R.R., Kanduri, M., Göndör, A., Grange, T., Ohlsson, R., and Kanduri, C. (2004). An antisense RNA regulates the bidirectional silencing property of the Kcnq1 imprinting

control region. Mol. Cell Biol. *24*, 7855–7862. https://doi.org/10.1128/MCB.24.18.7855-7862.2004.

25. Sleutels, F., Zwart, R., and Barlow, D.P. (2002). The non-coding Air RNA is required for silencing autosomal imprinted genes. Nature *415*, 810–813. https://doi.org/10.1038/415810a.
26. Luo, S., Lu, J.Y., Liu, L., Yin, Y., Chen, C., Han, X., Wu, B., Xu, R., Liu, W., Yan, P., et al. (2016). Divergent lncRNAs regulate gene expression and lineage differentiation in pluripotent cells. Cell Stem Cell *18*, 637–652. https://doi.org/10.1016/j.stem.2016.01.024.
27. Feng, J., Bi, C., Clark, B.S., Mady, R., Shah, P., and Kohtz, J.D. (2006). The Evf-2 noncoding RNA is transcribed from the Dlx-5/6 ultraconserved region and functions as a Dlx-2 transcriptional coactivator. Genes Dev. *20*, 1470–1484. https://doi.org/10.1101/gad.1416106.
28. Engström, P.G., Suzuki, H., Ninomiya, N., Akalin, A., Sessa, L., Lavorgna, G., Brozzi, A., Luzi, L., Tan, S.L., Yang, L., et al. (2006). Complex Loci in human and mouse genomes. PLoS Genet. *2*, e47. https://doi.org/10.1371/journal.pgen.0020047.
29. Statello, L., Guo, C.J., Chen, L.L., and Huarte, M. (2021). Gene regulation by long non-coding RNAs and its biological functions. Nat. Rev. Mol. Cell Biol. *22*, 96–118. https://doi.org/10.1038/s41580-020-00315-9.
30. Melé, M., Mattioli, K., Mallard, W., Shechner, D.M., Gerhardinger, C., and Rinn, J.L. (2017). Chromatin environment, transcriptional regulation, and splicing distinguish lincRNAs and mRNAs. Genome Res. *27*, 27–37. https://doi.org/10.1101/gr.214205.116.
31. Zuckerman, B., and Ulitsky, I. (2019). Predictive models of subcellular localization of long RNAs. RNA *25*, 557–572. https://doi.org/10.1261/rna.068288.118.
32. Guttman, M., Amit, I., Garber, M., French, C., Lin, M.F., Feldser, D., Huarte, M., Zuk, O., Carey, B.W., Cassady, J.P., et al. (2009). Chromatin signature reveals over a thousand highly conserved large non-coding RNAs in mammals. Nature *458*, 223–227. https://doi.org/10.1038/nature07672.
33. Guttman, M., Donaghey, J., Carey, B.W., Garber, M., Grenier, J.K., Munson, G., Young, G., Lucas, A.B., Ach, R., Bruhn, L., et al. (2011). lincRNAs act in the circuitry controlling pluripotency and differentiation. Nature *477*, 295–300. https://doi.org/10.1038/nature10398.
34. Derrien, T., Johnson, R., Bussotti, G., Tanzer, A., Djebali, S., Tilgner, H., Guernec, G., Martin, D., Merkel, A., Knowles, D.G., et al. (2012). The GENCODE v7 catalog of human long noncoding RNAs: analysis of their gene structure, evolution, and expression. Genome Res. *22*, 1775–1789. https://doi.org/10.1101/gr.132159.111.
35. Tian, B., and Manley, J.L. (2017). Alternative polyadenylation of mRNA precursors. Nat. Rev. Mol. Cell Biol. *18*, 18–30. https://doi.org/10.1038/nrm.2016.116.
36. Guo, C.J., Ma, X.K., Xing, Y.H., Zheng, C.C., Xu, Y.F., Shan, L., Zhang, J., Wang, S., Wang, Y., Carmichael, G.G., et al. (2020). Distinct processing of lncRNAs contributes to non-conserved functions in stem cells. Cell *181*, 621–636.e22. https://doi.org/10.1016/j.cell.2020.03.006.
37. Gil, N., and Ulitsky, I. (2020). Regulation of gene expression by cis-acting long non-coding RNAs. Nat. Rev. Genet. *21*, 102–117. https://doi.org/10.1038/s41576-019-0184-5.
38. Akhade, V.S., Pal, D., and Kanduri, C. (2017). Long noncoding RNA: genome organization and mechanism of action. Adv. Exp. Med. Biol. *1008*, 47–74. https://doi.org/10.1007/978-981-10-5203-3_2.
39. Fitzpatrick, G.V., Soloway, P.D., and Higgins, M.J. (2002). Regional loss of imprinting and growth deficiency in mice with a targeted deletion of KvDMR1. Nat. Genet. *32*, 426–431. https://doi.org/10.1038/ng988.
40. Mak, W., Baxter, J., Silva, J., Newall, A.E., Otte, A.P., and Brockdorff, N. (2002). Mitotically stable association of polycomb group proteins eed and enx1 with the inactive x chromosome in trophoblast stem cells. Curr. Biol. *12*, 1016–1020. https://doi.org/10.1016/s0960-9822(02)00892-8.
41. Plath, K., Fang, J., Mlynarczyk-Evans, S.K., Cao, R., Worringer, K.A., Wang, H., de la Cruz, C.C., Otte, A.P., Panning, B., and Zhang, Y. (2003). Role of histone H3 lysine 27 methylation in X inactivation. Science *300*, 131–135. https://doi.org/10.1126/science.1084274.
42. Silva, J., Mak, W., Zvetkova, I., Appanah, R., Nesterova, T.B., Webster, Z., Peters, A.H.F.M., Jenuwein, T., Otte, A.P., and Brockdorff, N. (2003). Establishment of histone h3 methylation on the inactive X chromosome requires transient recruitment of Eed-Enx1 polycomb group complexes. Dev. Cell *4*, 481–495. https://doi.org/10.1016/s1534-5807(03)00068-6.
43. Pandey, R.R., Mondal, T., Mohammad, F., Enroth, S., Redrup, L., Komorowski, J., Nagano, T., Mancini-Dinardo, D., and Kanduri, C. (2008). Kcnq1ot1 antisense noncoding RNA mediates lineage-specific transcriptional silencing through chromatin-level regulation. Mol. Cell *32*, 232–246. https://doi.org/10.1016/j.molcel.2008.08.022.
44. Zhao, J., Ohsumi, T.K., Kung, J.T., Ogawa, Y., Grau, D.J., Sarma, K., Song, J.J., Kingston, R.E., Borowsky, M., and Lee, J.T. (2010). Genome-wide identification of polycomb-associated RNAs by RIP-seq. Mol. Cell *40*, 939–953. https://doi.org/10.1016/j.molcel.2010.12.011.
45. Zhao, J., Sun, B.K., Erwin, J.A., Song, J.J., and Lee, J.T. (2008). Polycomb proteins targeted by a short repeat RNA to the mouse X chromosome. Science *322*, 750–756. https://doi.org/10.1126/science.1163045.
46. Kanhere, A., Viiri, K., Araújo, C.C., Rasaiyaah, J., Bouwman, R.D., Whyte, W.A., Pereira, C.F., Brookes, E., Walker, K., Bell, G.W., et al. (2010). Short RNAs are transcribed from repressed polycomb target genes and interact with polycomb repressive complex-2. Mol. Cell *38*, 675–688. https://doi.org/10.1016/j.molcel.2010.03.019.
47. Beckedorff, F.C., Ayupe, A.C., Crocci-Souza, R., Amaral, M.S., Nakaya, H.I., Soltys, D.T., Menck, C.F.M., Reis, E.M., and Verjovski-Almeida, S. (2013). The intronic long noncoding RNA ANRASSF1 recruits PRC2 to the RASSF1A promoter, reducing the expression of RASSF1A and increasing cell proliferation. PLoS Genet. *9*, e1003705. https://doi.org/10.1371/journal.pgen.1003705.
48. Redrup, L., Branco, M.R., Perdeaux, E.R., Krueger, C., Lewis, A., Santos, F., Nagano, T., Cobb, B.S., Fraser, P., and Reik, W. (2009). The long noncoding RNA Kcnq1ot1 organises a lineage-specific nuclear domain for epigenetic gene silencing. Development *136*, 525–530. https://doi.org/10.1242/dev.031328.
49. Heo, J.B., and Sung, S. (2011). Vernalization-mediated epigenetic silencing by a long intronic noncoding RNA. Science *331*, 76–79. https://doi.org/10.1126/science.1197349.
50. Schertzer, M.D., Braceros, K.C.A., Starmer, J., Cherney, R.E., Lee, D.M., Salazar, G., Justice, M., Bischoff, S.R., Cowley, D.O., Ariel, P., et al. (2019). lncRNA-induced spread of polycomb controlled by genome architecture, RNA abundance, and CpG island DNA. Mol. Cell *75*, 523–537.e10. https://doi.org/10.1016/j.molcel.2019.05.028.
51. Davidovich, C., Wang, X., Cifuentes-Rojas, C., Goodrich, K.J., Gooding, A.R., Lee, J.T., and Cech, T.R. (2015). Toward a consensus on the binding specificity and promiscuity of PRC2 for RNA. Mol. Cell *57*, 552–558. https://doi.org/10.1016/j.molcel.2014.12.017.
52. Davidovich, C., Zheng, L., Goodrich, K.J., and Cech, T.R. (2013). Promiscuous RNA binding by Polycomb repressive complex 2. Nat. Struct. Mol. Biol. *20*, 1250–1257. https://doi.org/10.1038/nsmb.2679.
53. Wang, X., Goodrich, K.J., Gooding, A.R., Naeem, H., Archer, S., Paucek, R.D., Youmans, D.T., Cech, T.R., and Davidovich, C. (2017). Targeting of polycomb repressive complex 2 to RNA by short repeats of consecutive guanines. Mol. Cell *65*, 1056–1067.e5. https://doi.org/10.1016/j.molcel.2017.02.003.
54. Gowher, H., Stuhlmann, H., and Felsenfeld, G. (2008). Vezf1 regulates genomic DNA methylation through its effects on expression of DNA methyltransferase Dnmt3b. Genes Dev. *22*, 2075–2084. https://doi.org/10.1101/gad.1658408.
55. Jinawath, A., Miyake, S., Yanagisawa, Y., Akiyama, Y., and Yuasa, Y. (2005). Transcriptional regulation of the human DNA methyltransferase 3A and 3B genes by Sp3 and Sp1 zinc finger proteins. Biochem. J. *385*, 557–564. https://doi.org/10.1042/BJ20040684.

56. Ishida, C., Ura, K., Hirao, A., Sasaki, H., Toyoda, A., Sakaki, Y., Niwa, H., Li, E., and Kaneda, Y. (2003). Genomic organization and promoter analysis of the Dnmt3b gene. Gene *310*, 151–159.

57. Naumova, N., Smith, E.M., Zhan, Y., and Dekker, J. (2012). Analysis of long-range chromatin interactions using Chromosome Conformation Capture. Methods *58*, 192–203. https://doi.org/10.1016/j.ymeth.2012.07.022.

58. Hagège, H., Klous, P., Braem, C., Splinter, E., Dekker, J., Cathala, G., de Laat, W., and Forné, T. (2007). Quantitative analysis of chromosome conformation capture assays (3C-qPCR). Nat. Protoc. *2*, 1722–1733. https://doi.org/10.1038/nprot.2007.243.

59. Petell, C.J., Alabdi, L., He, M., San Miguel, P., Rose, R., and Gowher, H. (2016). An epigenetic switch regulates de novo DNA methylation at a subset of pluripotency gene enhancers during embryonic stem cell differentiation. Nucleic Acids Res. *44*, 7605–7617. https://doi.org/10.1093/nar/gkw426.

60. Yagi, M., Kabata, M., Tanaka, A., Ukai, T., Ohta, S., Nakabayashi, K., Shimizu, M., Hata, K., Meissner, A., Yamamoto, T., and Yamada, Y. (2020). Identification of distinct loci for de novo DNA methylation by DNMT3A and DNMT3B during mammalian development. Nat. Commun. *11*, 3199. https://doi.org/10.1038/s41467-020-16989-w.

61. Kim, G.D., Ni, J., Kelesoglu, N., Roberts, R.J., and Pradhan, S. (2002). Co-operation and communication between the human maintenance and de novo DNA (cytosine-5) methyltransferases. EMBO J. *21*, 4183–4195. https://doi.org/10.1093/emboj/cdf401.

62. Williamson, J.R., Raghuraman, M.K., and Cech, T.R. (1989). Monovalent cation-induced structure of telomeric DNA: the G-quartet model. Cell *59*, 871–880. https://doi.org/10.1016/0092-8674(89)90610-7.

63. Pintacuda, G., Wei, G., Roustan, C., Kirmizitas, B.A., Solcan, N., Cerase, A., Castello, A., Mohammed, S., Moindrot, B., Nesterova, T.B., and Brockdorff, N. (2017). hnRNPK recruits PCGF3/5-PRC1 to the xist RNA B-repeat to establish polycomb-mediated chromosomal silencing. Mol. Cell *68*, 955–969.e10. https://doi.org/10.1016/j.molcel.2017.11.013.

64. Smith, S.A., Ray, D., Cook, K.B., Mallory, M.J., Hughes, T.R., and Lynch, K.W. (2013). Paralogs hnRNP L and hnRNP LL exhibit overlapping but distinct RNA binding constraints. PLoS One *8*, e80701. https://doi.org/10.1371/journal.pone.0080701.

65. Hung, L.H., Heiner, M., Hui, J., Schreiner, S., Benes, V., and Bindereif, A. (2008). Diverse roles of hnRNP L in mammalian mRNA processing: a combined microarray and RNAi analysis. RNA *14*, 284–296. https://doi.org/10.1261/rna.725208.

66. Preussner, M., Schreiner, S., Hung, L.H., Porstner, M., Jäck, H.M., Benes, V., Rätsch, G., and Bindereif, A. (2012). HnRNP L and L-like cooperate in multiple-exon regulation of CD45 alternative splicing. Nucleic Acids Res. *40*, 5666–5678. https://doi.org/10.1093/nar/gks221.

67. Cole, B.S., Tapescu, I., Allon, S.J., Mallory, M.J., Qiu, J., Lake, R.J., Fan, H.Y., Fu, X.D., and Lynch, K.W. (2015). Global analysis of physical and functional RNA targets of hnRNP L reveals distinct sequence and epigenetic features of repressed and enhanced exons. RNA *21*, 2053–2066. https://doi.org/10.1261/rna.052969.115.

68. Bhattacharya, S., Wang, S., Reddy, D., Shen, S., Zhang, Y., Zhang, N., Li, H., Washburn, M.P., Florens, L., Shi, Y., et al. (2021). Structural basis of the interaction between SETD2 methyltransferase and hnRNP L paralogs for governing co-transcriptional splicing. Nat. Commun. *12*, 6452. https://doi.org/10.1038/s41467-021-26799-3.

69. Bhattacharya, S., Levy, M.J., Zhang, N., Li, H., Florens, L., Washburn, M.P., and Workman, J.L. (2021). The methyltransferase SETD2 couples transcription and splicing by engaging mRNA processing factors through its SHI domain. Nat. Commun. *12*, 1443. https://doi.org/10.1038/s41467-021-21663-w.

70. Yuan, W., Xie, J., Long, C., Erdjument-Bromage, H., Ding, X., Zheng, Y., Tempst, P., Chen, S., Zhu, B., and Reinberg, D. (2009). Heterogeneous nuclear ribonucleoprotein L Is a subunit of human KMT3a/Set2 complex required for H3 Lys-36 trimethylation activity in vivo. J. Biol. Chem. *284*, 15701–15707. https://doi.org/10.1074/jbc.M808431200.

71. Esteller, M. (2005). Aberrant DNA methylation as a cancer-inducing mechanism. Annu. Rev. Pharmacol. Toxicol. *45*, 629–656. https://doi.org/10.1146/annurev.pharmtox.45.120403.095832.

72. Watanabe, Y., and Maekawa, M. (2010). Methylation of DNA in cancer. Adv. Clin. Chem. *52*, 145–167.

73. Walton, E.L., Francastel, C., and Velasco, G. (2014). Dnmt3b prefers germ line genes and centromeric regions: lessons from the ICF syndrome and cancer and implications for diseases. Biology *3*, 578–605. https://doi.org/10.3390/biology3030578.

74. Shuman, S. (2020). Transcriptional interference at tandem lncRNA and protein-coding genes: an emerging theme in regulation of cellular nutrient homeostasis. Nucleic Acids Res. *48*, 8243–8254. https://doi.org/10.1093/nar/gkaa630.

75. Xiang, J.F., Yin, Q.F., Chen, T., Zhang, Y., Zhang, X.O., Wu, Z., Zhang, S., Wang, H.B., Ge, J., Lu, X., et al. (2014). Human colorectal cancer-specific CCAT1-L lncRNA regulates long-range chromatin interactions at the MYC locus. Cell Res. *24*, 513–531. https://doi.org/10.1038/cr.2014.35.

76. Yang, F., Deng, X., Ma, W., Berletch, J.B., Rabaia, N., Wei, G., Moore, J.M., Filippova, G.N., Xu, J., Liu, Y., et al. (2015). The lncRNA Firre anchors the inactive X chromosome to the nucleolus by binding CTCF and maintains H3K27me3 methylation. Genome Biol. *16*, 52. https://doi.org/10.1186/s13059-015-0618-0.

77. Saldana-Meyer, R., Rodriguez-Hernaez, J., Escobar, T., Nishana, M., Jacome-Lopez, K., Nora, E.P., Bruneau, B.G., Tsirigos, A., Furlan-Magaril, M., Skok, J., and Reinberg, D. (2019). RNA interactions are essential for CTCF-mediated genome organization. Mol. Cell *76*, 412–422.e415. https://doi.org/10.1016/j.molcel.2019.08.015.

78. Hui, J., Reither, G., and Bindereif, A. (2003). Novel functional role of CA repeats and hnRNP L in RNA stability. RNA *9*, 931–936. https://doi.org/10.1261/rna.5660803.

79. Ruan, X., Li, P., Cangelosi, A., Yang, L., and Cao, H. (2016). A long noncoding RNA, lncLGR, regulates hepatic glucokinase expression and glycogen storage during fasting. Cell Rep. *14*, 1867–1875. https://doi.org/10.1016/j.celrep.2016.01.062.

80. Atianand, M.K., Hu, W., Satpathy, A.T., Shen, Y., Ricci, E.P., Alvarez-Dominguez, J.R., Bhatta, A., Schattgen, S.A., McGowan, J.D., Blin, J., et al. (2016). A long noncoding RNA lincRNA-EPS acts as a transcriptional brake to restrain inflammation. Cell *165*, 1672–1685. https://doi.org/10.1016/j.cell.2016.05.075.

81. Li, Z., Chao, T.C., Chang, K.Y., Lin, N., Patil, V.S., Shimizu, C., Head, S.R., Burns, J.C., and Rana, T.M. (2014). The long noncoding RNA THRIL regulates TNFalpha expression through its interaction with hnRNPL. Proc. Natl. Acad. Sci. USA *111*, 1002–1007. https://doi.org/10.1073/pnas.1313768111.

82. Yin, Y., Lu, J.Y., Zhang, X., Shao, W., Xu, Y., Li, P., Hong, Y., Cui, L., Shan, G., Tian, B., et al. (2020). U1 snRNP regulates chromatin retention of noncoding RNAs. Nature *580*, 147–150. https://doi.org/10.1038/s41586-020-2105-3.

83. Shukla, C.J., McCorkindale, A.L., Gerhardinger, C., Korthauer, K.D., Cabili, M.N., Shechner, D.M., Irizarry, R.A., Maass, P.G., and Rinn, J.L. (2018). High-throughput identification of RNA nuclear enrichment sequences. EMBO J. *37*, e98452. https://doi.org/10.15252/embj.201798452.

84. Lubelsky, Y., and Ulitsky, I. (2018). Sequences enriched in Alu repeats drive nuclear localization of long RNAs in human cells. Nature *555*, 107–111. https://doi.org/10.1038/nature25757.

85. Hacisuleyman, E., Shukla, C.J., Weiner, C.L., and Rinn, J.L. (2016). Function and evolution of local repeats in the Firre locus. Nat. Commun. *7*, 11021. https://doi.org/10.1038/ncomms11021.

86. Huang, Y., Li, W., Yao, X., Lin, Q.J., Yin, J.W., Liang, Y., Heiner, M., Tian, B., Hui, J., and Wang, G. (2012). Mediator complex regulates alternative mRNA processing via the MED23 subunit. Mol. Cell *45*, 459–469. https://doi.org/10.1016/j.molcel.2011.12.022.

87. Cramer, P., Pesce, C.G., Baralle, F.E., and Kornblihtt, A.R. (1997). Functional association between promoter structure and transcript alternative splicing. Proc. Natl. Acad. Sci. USA *94*, 11456–11460. https://doi.org/10.1073/pnas.94.21.11456.

88. Gowher, H., Brick, K., Camerini-Otero, R.D., and Felsenfeld, G. (2012). Vezf1 protein binding sites genome-wide are associated with pausing of elongating RNA polymerase II. Proc. Natl. Acad. Sci. USA *109*, 2370–2375. https://doi.org/10.1073/pnas.1121538109.

89. Hahm, B., Cho, O.H., Kim, J.E., Kim, Y.K., Kim, J.H., Oh, Y.L., and Jang, S.K. (1998). Polypyrimidine tract-binding protein interacts with HnRNP L. FEBS Lett. *425*, 401–406. https://doi.org/10.1016/s0014-5793(98)00269-5.

90. AlAbdi, L., Saha, D., He, M., Dar, M.S., Utturkar, S.M., Sudyanti, P.A., McCune, S., Spears, B.H., Breedlove, J.A., Lanman, N.A., and Gowher, H. (2020). Oct4-Mediated inhibition of Lsd1 activity promotes the active and primed state of pluripotency enhancers. Cell Rep. *30*, 1478–1490.e6. https://doi.org/10.1016/j.celrep.2019.11.040.

91. Panda, A.C., Martindale, J.L., and Gorospe, M. (2016). Affinity pull-down of biotinylated RNA for detection of protein-RNA complexes. Bio. Protoc. *6*, e2062. https://doi.org/10.21769/BioProtoc.2062.

92. Wuarin, J., and Schibler, U. (1994). Physical isolation of nascent RNA chains transcribed by RNA polymerase II: evidence for cotranscriptional splicing. Mol. Cell Biol. *14*, 7219–7225. https://doi.org/10.1128/mcb.14.11.7219-7225.1994.

93. Pandya-Jones, A., and Black, D.L. (2009). Co-transcriptional splicing of constitutive and alternative exons. RNA *15*, 1896–1908. https://doi.org/10.1261/rna.1714509.

94. Chu, C., Quinn, J., and Chang, H.Y. (2012). Chromatin isolation by RNA purification (ChIRP). JoVE, e3912. https://doi.org/10.3791/3912.

95. Tremblay, K.D., Duran, K.L., and Bartolomei, M.S. (1997). A 5' 2-kilobase-pair region of the imprinted mouse H19 gene exhibits exclusive paternal methylation throughout development. Mol. Cell Biol. *17*, 4322–4329.

96. Peach, M., Marsh, N., Miskiewicz, E.I., and MacPhee, D.J. (2015). Solubilization of proteins: the importance of lysis buffer choice. Methods Mol. Biol. *1312*, 49–60. https://doi.org/10.1007/978-1-4939-2694-7_8.

97. Shevchenko, A., Tomas, H., Havlis, J., Olsen, J.V., and Mann, M. (2006). In-gel digestion for mass spectrometric characterization of proteins and proteomes. Nat. Protoc. *1*, 2856–2860. https://doi.org/10.1038/nprot.2006.468.

STAR★METHODS

KEY RESOURCES TABLE

REAGENT or RESOURCE	SOURCE	IDENTIFIER
Antibodies		
anti- H3K27Ac	Active Motif	Cat# 39133, RRID:AB_2561016)
anti-hnRNPL	Abcam	Cat# ab32680, RRID:AB_941986
anti-Dnmt3b	Abcam	Cat# ab13604, RRID:AB_300494
anti-GAPDH	Santa Cruz	Cat# sc47724, RRID:AB_627678
anti-SSEA-1	R and D Systems	Cat# MAB430, RRID:AB_2208782
anti-AlexaFluor 555 nm	Molecular Probes	Cat# A-21422, RRID:AB_141822
anti-H3K4me1	Active Motif	Cat# 39297, RRID:AB_2615075
anti-H3K27me3	Abcam	Cat# ab6002, RRID:AB_305237
anti-hnRNPK	Abclonal	Cat# A1701, RRID:AB_2763753
anti-beta-actin	Santa Cruz Biotechnology	Cat# sc-47778, RRID:AB_626632
anti-H3K36me3	Abcam	Cat# ab9050, RRID:AB_306966
anti-H3	Abcam	Cat# ab61251, RRID:AB_941952
Polycomb Group 2 (PRC2) Antibody Sampler Kit	Cell signaling technology	Cat# 62083
anti-Dnmt3a	Active Motif	Cat# 39206, RRID:AB_2722512
Bacterial and Virus Strains		
XL10 E. Coli strain	NEB	Cat# C3040
Chemicals, Peptides, and Recombinant Proteins		
TRIzol	Invitrogen	Cat# 15596018
DNAse	Roche (Sigma-Aldrich)	Cat# 4716728001
RNAse	Roche (Sigma-Aldrich)	Cat# 11119915001
Proteinase K	Worthington	Cat# LS004222
Protease Inhibitor Cocktail	Roche (Sigma-Aldrich)	Cat# 11697498001
Protein A magnetic beads	Life Technologies	Cat# 10002D
Protein G magnetic beads	Life Technologies	Cat# 10004D
Dynabeads™ MyOne™ Streptavidin C1	Life Technologies	Cat# 65001
RNeasy Mini Kit	Qiagen	Cat# 74104
Verso One-Step RT-qPCR kit	Thermo Scientific	Cat# AB4105C
Tetro cDNA Synthesis Kit	Meridian Bioscience	Cat# BIO-65043
Lipofectamine 2000	Thermofischer	Cat# 11668019
Lipofectamine 3000	Thermofischer	Cat# L3000008
Lipofectamine™ RNAiMAX	Thermofischer	Cat# 13778030
Dynabeads™ MyOne™ Streptavidin C1	Thermofischer	Cat# 65001
Dynabeads™ M-280 Streptavidin	Thermofischer	Cat# 11205D
Protector Rnase Inhibitor	Sigma Aldrich	Cat# 3335399001
MEGAscript™ T7 Transcription Kit	Thermofisher	Cat# AM1333
Experimental Models: Cell Lines		
E14Tg2A Embryonic stem cells	MMRRC	Cat# 015890-UCD
Oligonucleotides		
Primers	This Manuscript	Table S1
ChIRP probes	This Manuscript	Table S2
Recombinant DNA		
pLKO.1 - TRC Cloning Vector	Addgene	Cat# 10878
Software and Algorithms		
G-quadruplex analysis tool	QGRS Mapper	https://bioinformatics.ramapo.edu/QGRS/index.php

RESOURCE AVAILABILITY

Lead contact

Further information and requests for resources and reagents should be directed to and will be fulfilled by the lead contact, Humaira Gowher (hgowher@purdue.edu).

Materials availability

Newly generated materials associated with the paper, including *Dnmt3bas* plasmids, are available upon a written request to the lead contact and must fill the MTA requirements of Purdue University.

Data and code availability

The raw qPCR data for gene expression, ChIP, and ChIRP will be shared by the lead contact upon request. Microscopy data reported in this paper will be shared by the lead contact upon request.

This paper does not report any original code.

Any additional information required to reanalyze the data reported in this paper is available from the lead contact upon request.

EXPERIMENTAL MODEL AND STUDY PARTICIPANT DETAILS

All the experiments were performed *in vitro* using authenticated male mouse embryonic stem cells, E14Tg2A, purchased at passage 12 from MMRRC. The mouse strain used for this research project, ES Parental cell line E14Tg2a.4, RRID:MMRRC_015890-UCD, was obtained from the Mutant Mouse Resource and Research Center (MMRRC) at University of California at Davis, an NIH-funded strain repository, and was donated to the MMRRC by BayGenomics, BayGenomics Consortium (https://www.mmrrc.org/catalog/cellLineSDS.php?mmrrc_id=15890). The ESCs were propagated and frozen at P14. Cells at P14 were thawed and adapted to 2i medium conditions for 7–9 passages. All experiments were performed in 2i-adapted cells at P9-12 or serum-cultivated ESCs at P16-18. The details of the culture condition are Method Details.

METHOD DETAILS

Cell culture and transgenic cell lines

1. ESC culture and differentiation

E14Tg2A (WT) ESCs were maintained in ESC media containing LIF on gelatin-coated tissue as described in https://www.mmrrc.org/strains/E14/Ctr_protocol.pdf. Differentiation of mESCs was induced by plating $10X10^6$ cells in low attachment 10 cm Petri dishes with a concurrent withdrawal of LIF. After Day 3, embryoid bodies were treated with 1μM Retinoic acid (RA), the medium was replenished daily, cells were harvested daily, and samples were collected for protein, RNA, DNA, and chromatin until Day 9.

2. 2i adaptation

Serum-mESCs were seeded in a T-25 flask and passaged once before adapting them into 2i media. Briefly, the serum-mESCs were washed with PBS and detached with trypsin. FBS was added to inactivate the trypsin, DMEM/F12 media was added, and cells were pelleted. The cells were rewashed to remove any traces of FBS and then plated and grown on gelatin-coated tissue culture plates in 2i media (3μM CHIR99021 and 1μM PD0325901). The cells were adapted until passage 10, and at every passage, the cells were harvested and checked for gene expression and DNA methylation. The differentiation was induced by removing LIF from the media, and at D3, 1μM RA was added, as explained earlier. The cells were harvested at different time points for the analysis.

3. Transgenic cell lines

CRISPR KO *dnmt3a* cell lines were a gift from Dr. Taiping Chen, MD Anderson. Transgenic *Dnmt3bas* knockdown (KD) and overexpression (OE) cell lines were generated by transfecting serum-cultured ESCs with pLKO.1 shRNA (Dharmacon) and pcDNA3.1*Dnmt3bas* (spliced and unspliced). pcDNA3.1GFP transfected cells were used as control. After antibiotic selection, the derived stable cell lines were adapted to the 2i culture conditions described below. For hnRNPL knockdown, serum-cultured OE cells were treated with siRNA hnRNPL (Thermo Fischer) for 48 h, and RNA was purified for expression analysis.

Microscopy

Bright-field images of s-ESCs and 2i-ESCs were obtained with a Zeiss microscope using a 10×591 objective. We performed Alkaline phosphatase staining and SSEA-1 staining in these cells, as previously reported.[90] Briefly, the cells were stained with alkaline phosphatase (Sigma, AB0300) and SSEA-1 staining using (Millipore, 597 MAB430) and Alexa Fluor 555 nm (Life Technologies, A21422) antibodies. The SSEA-1 and Alkaline 598 phosphatase stained cells were imaged using 20X objectives under Nikon Ts and Zeiss 599 microscopes, respectively.

RT-qPCR and RT-PCR

1. Gene expression

Briefly, total RNA was isolated using the TRIzol reagent (Invitrogen, 15596026) according to the manufacturer's protocol. First, RNA samples were digested with DNAse (Roche, 04716728001) at 37°C for 2 h and purified using a Quick-RNA MiniPrep Plus Kit (ZymoReseach, R1057). Then, reverse-transcription quantitative PCR (RT-qPCR) was performed either using Verso One-Step RT-qPCR kits (Thermo Scientific, AB-4104A) or by two-step method in which cDNA was synthesized using the Tetro cDNA Synthesis Kit (Bioline, BIO-65043). For Verso One-Step RT-qPCR, we used 5-50ng of RNA per reaction; for the two-step method, we used 1.2–2.5μg of RNA to synthesize cDNA. cDNA was synthesized using gene-specific primers (GSP), random hexamers, or oligo (dT) per the manufacturer's instructions. Gene expression was calculated as $\Delta C_{t,}$ which is C_t(Gene)- C_t(*Gapdh or Beta-actin*). Change in gene expression is reported as fold change relative to control undifferentiated cells, which was set to 1, or in a $\log_2$ scale where values of undifferentiated cells were set to 0. Standard deviations represent at least 2 technical and 2 biological replicates. SEM represents the variance in average data with n = 6 or more. The SD, SEM determination, and p-Value were calculated using GraphPad Prism using ANOVA or paired Student T test.

2. Alternative splicing

To analyze alternative splicing, a 1-step RT-PCR kit (Invitrogen). We designed primers at exon-exon boundaries such that product sizes were 200–500 bps long, which were visualized on 6% Polyacrylamide gels in TBE buffer. Table S1 details the list of primers used in this study.

Chromosome conformation capture assay (3C)

3C assays followed the protocol from[57,58] with a few modifications. Murine 2i cells were crosslinked with 1% formaldehyde for 10 min at room temperature. Chromatin was suspended in NEB buffer 2.1 and digested with 1000 units of HaeIII at 37°C overnight. Crosslinked fragments were ligated with 45 units of T4 DNA ligase at 16°C for 2 h. A random ligation control template was generated using a BAC clone RP23-474F18 covering the *Dnmt3b* locus and digested with HaeIII and ligated with T4 ligase. Gapdh locus was used as an endogenous control. A standard for known concentrations of E14 genomic DNA was generated by qPCR with primer pair GaploadF and GaploadR and used to determine 3C samples concentration. The qPCR used the same amount of each 3C sample to determine the interaction frequency between the anchor fragment (F1) and the distant fragment. Each quantitative PCR reaction was triplicated using 3C and BAC samples as a template and 3C primers. Primer position and sequence are indicated in (Figure 1) and Table S1. The relative interaction frequency of each fragment to anchor was calculated as $2^{(Ct\ BAC\ -Ct\ 3C)}$. p-values were calculated using GraphPad Prism using paired Student T test.

RNA-pulldown and hnRNPL binding assays

The WT and mutant *Dnmt3bas* templates for *in vitro* transcription assays were obtained by PCR using primers containing the T7 promoter sequence (View primer list). Biotin-labeled *Dnmt3bas* transcripts, *Dnmt3bas* antisense, and *Dntm3bas* variants 1, 2, and 3 were transcribed *in vitro* using the T7 RNA polymerase (ThermoFisher Scientific, AM1333) with the following modifications. Unlabeled ATP, GTP, and CTP were used at a concentration of 7.5 mM, except for unlabeled UTP, which was used at 5.63 mM. Notably, the reaction was supplemented with 1.8 mM biotin-UTP (Roche, 11093070910). The transcripts were immobilized on streptavidin beads and incubated with pre-cleared nuclear extract from 2i-ESCs for 45 min at 4°C. Following washes, magnetic beads were boiled for 5 min in the SDS-loading buffer as previously described.[91] Eluates were analyzed using Coomassie staining and Western blot.

Subcellular fractionation

$20x10^6$ mESCs were harvested for the subcellular fractionation, according to the previously described[92,93] protocol. Briefly, the cells were trypsinized and centrifuged at low speed at RT for 5min. Cells were lysed by adding the NP-40 lysis buffer for 5 min. The samples were centrifuged, and the supernatant was saved as the cytosolic fraction. The pellet was rinsed with the lysis buffer to remove any cytoplasmic components. The pellet was then resuspended in glycerol buffer by gentle flicking, followed by the addition of nuclei lysis buffer. After 2 min of incubation, the sample was centrifuged, and the supernatant was collected as the soluble nuclear fraction/nucleoplasm. Part of the fraction was used to perform the Western blot, and the remaining fraction was used to isolate the RNA for RT-qPCR analysis.

Chromatin isolation by RNA purification (ChIRP)

Chromatin Isolation by RNA Purification (ChIRP) was performed by following.[94] Briefly >20 million cells were grown and crosslinked 1% glutaraldehyde at room temperature, followed by quenching for 5 min. The cell pellets were flash-frozen in liquid nitrogen and stored at −80°C indefinitely. The cells were thawed at room temperature and dislodged. For 100mg of cell pellet, we used 1mL of lysis buffer containing Protease Inhibitor cocktail, PMSF, and SUPERase•In RNase Inhibitor (Invitrogen). The cells were sonicated using a Bioruptor (Diagnode) in 15 mL tubes for 2–3 h. The sonicated sample was centrifuged, and the supernatant was hybridized with the biotinylated DNA probes specific to lncRNA, *Dnmt3bas*, for 4 h. In the meantime, C-1 magnetic beads were washed and added to the probe-sample mix. The complex was incubated at 37°C for 30 min and then washed 5 times with the 1mL wash buffer. The beads were resuspended in the final wash, and 100ul of the sample was kept for RNA purification. The complex was processed

accordingly for the downstream analysis. For RNA purification, the bead complex was resuspended in TriZol, and for DNA isolation, the complex was reverse crosslinked and RNase treated. RNA samples were used to measure the fold recovery of *Dnmt3bas* lncRNA by RT-qPCR. The purified ChIRP-DNA was used as a template to determine the enrichment of the genomic region of interest by qPCR. The bead complex was treated with a biotin elution buffer to isolate proteins[94] and immunoblotted to identify proteins of interest. Table S2 lists sequences of probes used in this study.

DNA methylation analysis

1. DNA methylation-dependent qPCR assay (MD-qPCR)

Genomic DNA (gDNA) was purified using the standard phenol-chloroform method. The extracted gDNA was treated with RNAse (Roche) overnight at 37°C. Following another round of Phenol-Chloroform DNA extraction, gDNA was subjected to FspE1 (NEB, R0662S) digestion overnight at 37°C. The digested gDNA was purified by the Phenol-Chloroform method and quantified using the NanoDrop 3300 fluorospectrometer through PicoGreen dye according to the manufacturer's protocol (Life Technologies, P11495). Quantitative PCR was performed using an equal amount of DNA for each sample. The change in DNA methylation is represented by relative fold change in the Cq value as follows: 2^(Cq(U)-Cq(I)), where Cq(U) is the Cq for the undifferentiated ESC sample, and Cq(I) represents day 3 or day 7 differentiated ESCs. The primers used for DNA methylation-dependent qPCR analysis have been previously described [30]. Standard deviations represent three technical and two biological replicates.

DNA Methylation-Dependent Restriction digest (MDR): Purified genomic DNA was subjected to methylation-sensitive restriction by Hpa II and methylation-insensitive restriction by Msp I overnight at 37°C. Samples were loaded on 0.8% Agarose gel in TAE buffer and bands visualized by Ethidium bromide staining. A smear in the Hpa II digestion lane indicates global loss of DNA methylation.

2. Bisulfite sequencing

Bisulfite sequencing was performed by using the EpiTect Fast Bisulfite Conversion Kit (Qiagen, 59802) according to the manufacturer's protocol. Bisulfite-converted DNA was PCR-amplified using published methods[95] and sequenced using Illumina Wide-SEQ run, which generated over 5K paired-end reads for each sample. The reads were then mapped by Bowtie2 and analyzed by Bismark for DNA methylation. Instances of methylated and unmethylated CpG were quantified and summed to an overall percent methylation for each gene with standard deviations. See Table S1 for primers used for bisulfite sequencing. Tables S3 and S4 give amplicon size, number of CpGs in the amplicon, and total reads used to determine %CpG methylation. The significance was calculated by the Wilcoxon matched-pairs rank test using GraphPad Prism.

3. Global DNA methylation using methylation-dependent restriction enzyme digestion

Genomic DNA was isolated using the standard phenol-chloroform method. Following RNase digestion and re-purification by phenol-chloroform, 1 μg of DNA was digested with either HpaII or MspI overnight at 37°C. As a control, 1 μg of DNA was incubated with digestion buffer under same conditions. Undigested and digested DNA samples were run on a 1% agarose Tris-acetic acid EDTA gel for 90 min at a constant 100 V. Following ethidium bromide staining, the gel was imaged with Axygen gel documentation system (Corning, GD-1000).

Chromatin immunoprecipitation

ChIP was performed as described.[59] Briefly, nuclei were isolated from the x-linked cells and were sonicated using Bioruptor (Diagnode), according to the manufacturer's protocol. A total of 8μg of sheared crosslinked chromatin was incubated with 8μg of antibody pre-loaded on a 1:1 ratio of protein A and protein G magnetic beads (Life Technologies, 10002D and 10004D, respectively). After washing the beads, the samples were eluted in 1% SDS, 10 mM EDTA, 50 mM Tris-HCl, pH 8.0. Crosslinking was reversed by incubation at 65°C for 30 min with shaking. Samples were treated with RNase (Roche, 11119915001) for 2 h at 37°C and then treated with Proteinase K (Worthington, LS004222) for 2 h at 55°C. DNA was purified by phenol: chloroform extraction followed by ethanol precipitation and quantified using PicoGreen (Life Technologies, P11495) and NanoDrop 3300 fluoro spectrometer. qPCR and data analysis were performed as previously described.[59] Enrichment was calculated as follows = Ct (IN)-Ct (IP) and the fold enrichment over input = 2^ [Ct (IN)-Ct (IP)]. Fold change was calculated by normalizing the fold enrichment at a specific site to that at the control region (Chr 17: 13821873–13821988). The significance of the change was determined via p value, which was calculated by GraphPad Prism using Student's t-test. Table S4 lists sequences of primers used.

Western blot

Standard Western blot analysis was conducted on nuclear protein extracts and RNA-pulldown eluates using anti-hnRNP L, 1:1000 (Abcam, ab32680), anti-hnRNP K, 1:1000 (Abclonal, A1701), and anti-rabbit, 1:40,000 (Jackson Immunoresearch, 111-035-003). Chemiluminescence was performed according to the manufacturer's protocol (Thermo-Fisher Scientific 34580). For DNMT3B expression, protein samples were purified using standard RIPA protein purification[96] and blotted using anti-Dnmt3b antibodies (sc-20704) and β-actin (sc-47778) as a loading control. Images were taken using the ChemiDoc MP imaging system (Biorad, 170001402).

RNA-Fluorescent in-situ hybridization assay (RNA-FISH)

ESCs were seeded on 0.1% gelatin-coated coverslips in a 24-well plate. After 24 h, cells were processed as per Stellaris RNA-FISH protocol for adherent cells. Briefly, cells were gently washed with 1X PBS and fixed with 3:1 methanol-glacial acetic acid fixation

buffer at room temperature for 10 min. Following fixation, cells were washed with Wash Buffer A (Biosearch Technologies, SMF-WA1-60) at room temperature for 5 min. Next, coverslips, cells side down, were transferred onto 100 μL of Hybridization buffer (Biosearch Technologies, cat# SMF-HB1-10) containing RNA probe within the humidified chamber. The following RNA probes were used – mouse *Gapdh* with Quasar 570 dye (Biosearch Technologies, SMF-3002-1) and a custom probe for mouse *Dnmt3bas* with Quasar 570 dye (Biosearch Technologies). For the *Dnmt3bas* probe set, 27 probes were designed using StellarisTM Probe Designer version 2.0. After overnight incubation in the dark at 37°C, coverslips were transferred back to a 24-well plate, cells side up, containing Wash Buffer A and incubated in the dark at 37°C. After 30 min, fresh Wash Buffer A containing Hoechst (Fisher Scientific, H3570) at 1:2000 dilution was added, and cells were incubated in the dark at 37°C for 30 min. After Hoechst staining, cells were washed in Wash Buffer B (Biosearch Technologies, SMF-WB1-20) for 5 min at room temperature. The coverslips were mounted in 25 μL of Prolong Glass Antifade Mountant (ThermoFisher Scientific, P36982) on a glass slide, and the samples were imaged the next day. Images were acquired using a Nikon A1R-MP microscope with a 60X oil objective (Nikon, Inc.). Nikon NIS-Elements imaging software (version 5.20.02) was used to acquire images in '.nd2' format and for further analysis. The acquisition settings were 1 K × 1 K resolution (pixels) with a scanning frame rate of 1/16 s. All images were set to the same display lookup table (LUT) settings before exporting as '. TIFF files.

1. RNA fish signal quantification

Cytoplasm and nuclear regions of interest (ROI) were identified as guided by the Hoechst signal. First, the nuclear signal was quantified as the cumulative intensity of the RNA probe signal (Quasar 570 signal) in their specific ROIs. Then, the nuclear/cytosolic signal ratio was taken for unprobed, GAPDH-probed, and *Dnmt3bas*-probed cells, and the data was plotted after normalizing to unprobed samples. ROI identification and signal quantification were performed using Nikon NIS-Elements imaging software (version 5.20.02). The number of nuclei quantified for each sample is represented as dots in the boxplot – untreated (n = 2), GAPDH (n = 3), and *Dnmt3bas* (n = 7).

In-gel trypsin digestion and mass spectrometry

The RNA-pull-down protein eluates were resolved with SDS-PAGE, followed by Coomassie staining. The observed unique 60 kDa band in the *Dnmt3bas* pull-down lane, which was absent in anti-sense *Dnmt3bas* lane was excised together with the corresponding region in the control lane. Proteins in the excised gel were destained and in-gel trypsin digested to obtain peptides as previously described.[97] The peptides were reconstituted in 50% acetonitrile/0.1% TFA and used for MALDI-TOF mass spectrometry to identify potential *Dnmt3bas* binding partners.

QUANTIFICATION AND STATISTICAL ANALYSIS

The details of the statistical analysis of various experiments can be found in the Methods details, figure legends, figures, and results. These details include the method of analysis, statistical tests, and the number of biological and technical repeats used for each experiment. Overall most analyses were performed using GraphPad Prism, and based on the experimental strategy, significance was determined using the Students T Test, ANOVA, or Wilcoxon -matched-pairs rank test.